ANALYSIS, SIMULATION AND MODELING OF THREE-LEVEL VSIs

by

Muhammet Cosan

A thesis submitted to the Faculty of the

Virginia Polytechnic Institute and State University

in partial fulfillment of the requirements for the degree of

MASTER OF SCIENCE

in

Electrical Engineering

Approved by:

Dr. Dusan Borojevic, Chairman

Dr. Fred C. Lee

Dr. Jason Lai

November 1997

Blacksburg, Virginia

ANALYSIS, SIMULATION AND MODELING OF THREE-LEVEL VSIs

by

Muhammet Cosan

Dusan Borojevic, Chairman

Electrical Engineering

(ABSTARCT)

Analysis of three-phase, three-level VSIs is done for high-power high-voltage applications. Complete Space Vector Modulation (SVM) algorithm is developed for a three-phase, three-level converter. Special attention is given to minimization of output ripple and voltage balance of the dc-link input capacitors. Verification of the proposed SVM algorithm is done by computer simulation. Comprehensive small-signal modeling of the three-level converter with a resistive load is developed the first time. Steady-state solutions reveal that the voltage across dc-link input capacitors is constant at the half of the dc-link voltage.

Acknowledgments

I would like to thank my advisor, Dusan Borojevic, for his invaluable support, understanding and encouragement. This work would not be possible without his esteemed guidance. I am also thankful to him for providing me with the opportunity to work at the Virginia Power Electronics Center (VPEC). It is a pleasure and an honor to be a VPEC graduate.

A great deal of credit for this work goes to my colleague Dr. Hengchun Mao. I would like to express my sincere gratitude to him for his help in this course of work. I also would like to thank Dr. Eng. Josep Bordonau, visiting scholar of Universitat Politecnica De Catalunya, Barcelona, Spain, for his valuable discussions and inputs especially in the modeling of the converters.

I am also grateful to Dr. Fred Lee, Dr. Dan Y. Chen, and Dr. Jason Lai whose teaching gave me a head start and a better understanding of power electronics. The completion of this thesis would not be possible without the valuable help given by friends Dong-Ho Lee and Heping Dai.

I am also thankful to all the departmental staff, and especially VPEC staff for their help during the course of this work. I am also grateful to Westinghouse Electric Co., for supporting this work.

Contents

List of Figures

List of Tables

1.INTRODUCTION

Three-phase multi-level voltage source inverters are suitable for high-voltage, high-power applications [1-2]. Their application in large motor drives and utility converters is expanding rapidly [3]. Fig. 1.1. shows an example of high-power application known as Superconductive Magnetic Energy Storage System (SMES), where shaded block represents the three-level voltage source inverter (VSI). Stored energy in superconductive coil is processed through the bidirectional chopper and three-level VSI. SMES system can be used to replace the high-power battery systems.

Fig. 1.2. shows the power stage of a three-level VSI. Similar to the three-level chopper [4], the voltage stress, switching loss and, inductor current ripple are all reduced in a multi-level inverter compared with a "two-level" inverter. However, the control of a three-level inverter is much more complex, due to the high number of switches and requirement of maintaining voltage balance between the upper half dc-link and the lower half dc link capacitors. Space Vector Modulation (SVM) algorithm for three-level VSI is proposed to determine the "on" times of power switches while maintaining a minimum output current ripple and minimum voltage swing of midpoint. Complete SVM algorithm is presented and SABER [5-6] simulation is performed to verify the SVM and the algorithm.

Accurate large and small signal models of inverter are required for control loop design. In this work, average and small signal models of a three-level VSI are presented for the first time. Unlike a conventional two-level VSI, three-level VSI has more control variables since there are total twelve switches.

In addition to controlling output active and reactive power, which is the case for a conventional two-level VSI, voltage across the input capacitors is chosen as the additional variable to control.

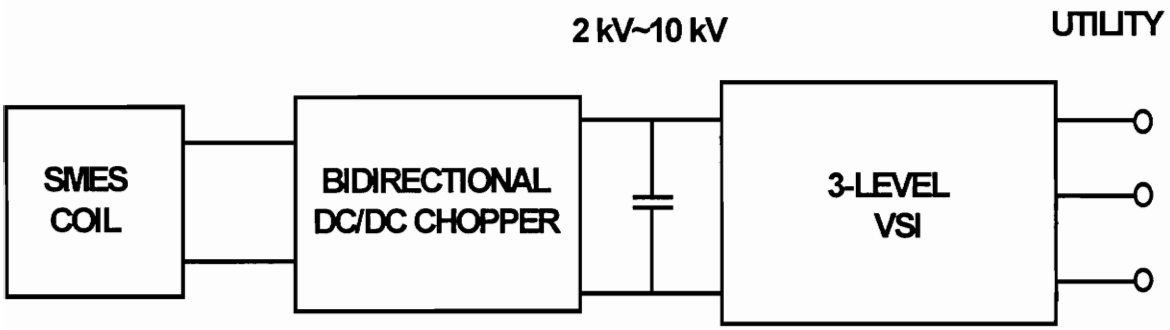

Fig. 1.1. Block diagram of a Superconductive Magnetic Energy Storage (SMES) system and three-level VSI

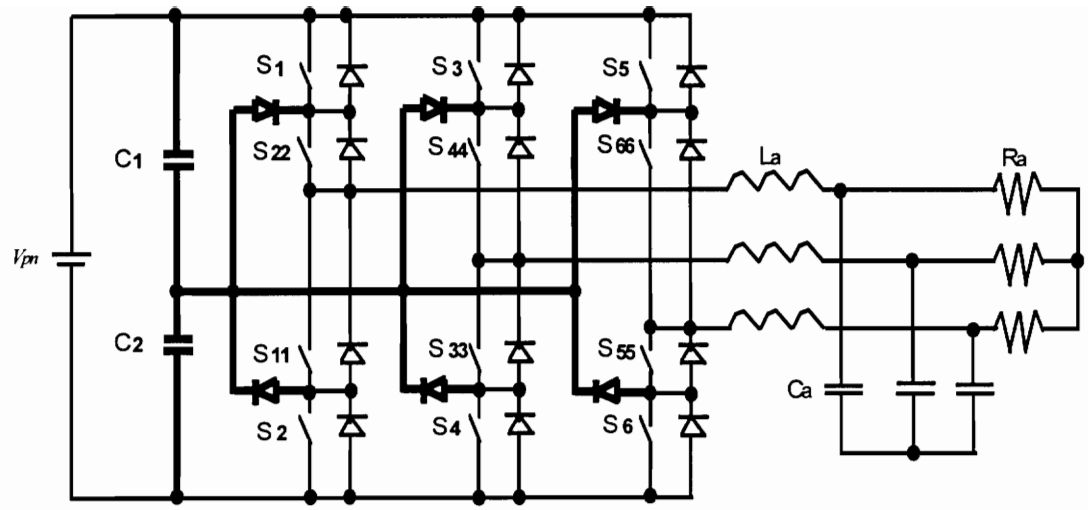

Fig. 1.2. Power stage of a three-level VSI

2. ANALYSIS OF THREE-LEVEL VSIs

2.1. Operation Principles

Each phase leg of the three-level VSI shown in Fig. 1.2 is composed of two upper and lower switches and their antiparallel diodes. Two input capacitors split the dc-bus voltage into two halves. In addition, six clamping diodes ensure that voltages across the switches will be determined by the voltages of the dc-link capacitors. The charge balance of the midpoint can be achieved by using a proper modulation scheme. Switching states for a three-level VSI must satisfy the following conditions:

- no shorting of the input capacitors, and
- continuity of the inductor current.

Fig. 2.1 (a) and (b) shows the two switching combinations of a three-level VSI. Notation "p", "o", and "n" means corresponding phase is connected to the positive rail, midpoint, and the negative rail, respectively. Note that, in addition to "p" and "n" states of the conventional two-level VSI, in three-level VSI a phase can be connected to the midpoint, "o" state. In Fig. 2.1 (a), line-to-line voltages are $v_{ab} = {Vpn}/{2}$, $v_{bc} = 0$, $v_{ca} = {-Vpn}/{2}$, and $i_o = -i_a$. On the other hand, in Fig. 2.1 (b), $v_{ab} = {Vpn}/{2}$, $v_{bc} = 0$, $v_{ca} = {-Vpn}/{2}$, and $i_o = i_a$. This kind of switching combinations produce the same output voltage but utilize the different dc-link capacitors and can be used for charge balance of the input capacitors.

Bidirectional power flow in a three-level VSI can be achieved by controlling the 12 switches. For a converter with 12 power switches, there are total 12^2 switching states. However, only 27 states satisfy the above conditions, and the rest of the states either short the input capacitors or open the output current path. Table 1 shows the relationship between the number of the switches, number of admissible switching combinations, number of free-wheeling states, so called zero vectors, and the level of the converter.

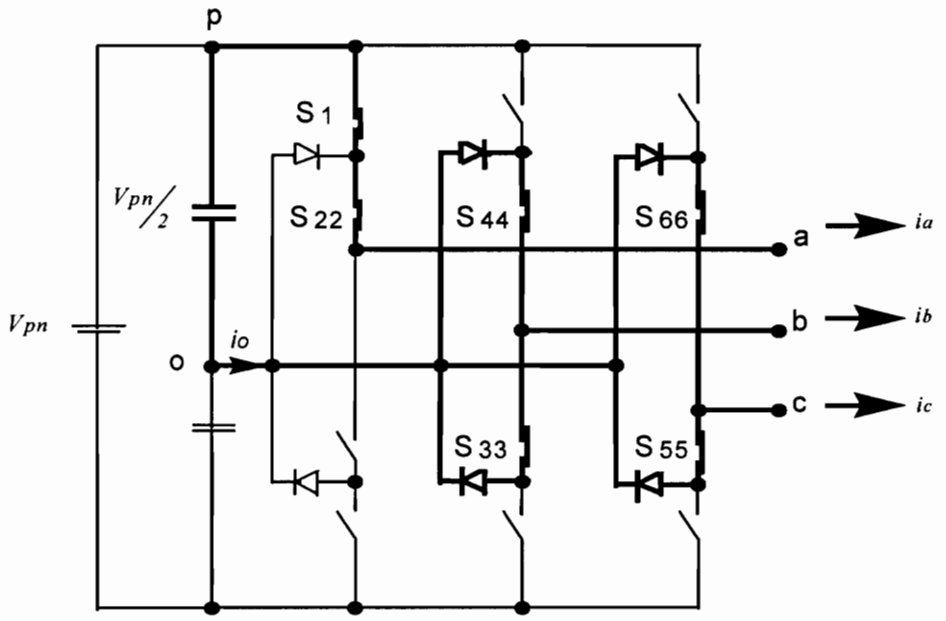

(a) poo state

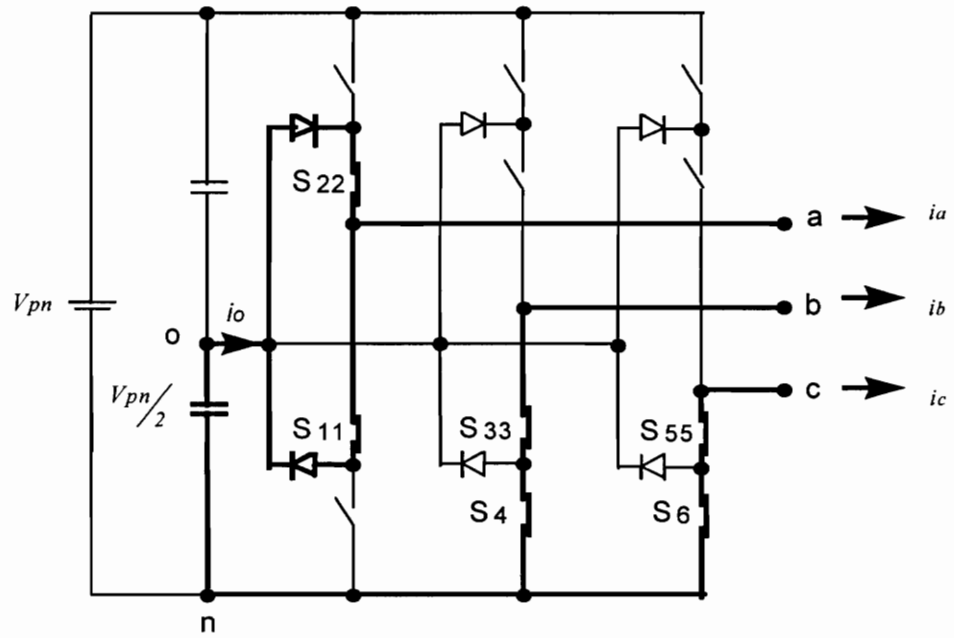

(b) onn state

Fig. 2.1. An example of switching states of a three-level VSI. Thick lines represent the active current path

Table 1 The relationship between level of a multi-level converter and number of switches, switching combinations, admissible states and free-wheeling states

	Number of Switches	Number of Switching Combinations	Number of Admissible Switching States	Num. of Free Wheeling States
2-level	6	6^2	8	2
3-level	12	12^2	27	3
4-level	18	18^2	64	4
m-level	$n = (m-1) \cdot 6$	n^2	m^3	m

To illustrate the difference between conventional two-level VSI and three-level VSI from the output voltage point of view, Fig. 2.2. presents the line-to-line voltages for both converters. It can be observed that, voltages in three-level VSI are more close to pure sine wave and have smaller ripple. In addition, switches are turned on and off with half of the bus voltage, $V_{pn}/2$, which reduces the switching loss and stress significantly.

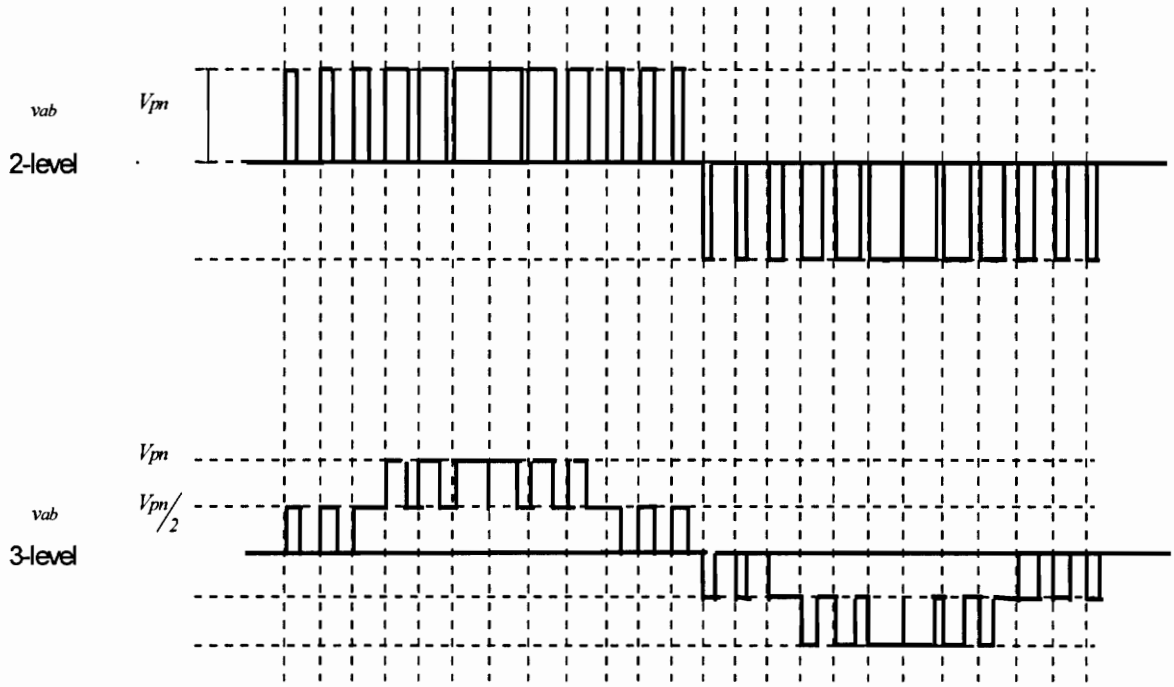

Fig. 2.2. Line-to-line voltages of two-level and three-level VSIs

2.2. Switching Function of Three-Level VSIs

Complex switching converters are analyzed by using switching functions which are discontinuous function of time taking values of "0" and "1" representing "off" and "on" states of the corresponding switches, respectively [7]. Fig. 2.3. shows the one leg of the conventional two-level VSI. Two switches and diodes in one leg are represented by a single-pole-double-throw switch. Ports connected to capacitors or voltage sources are chosen as throws, i.e. th1 and th2, and ports connected to inductor or current source are chosen as poles [8]. Fig. 2.4. shows the single-pole-double-throw switch representation of a conventional two-level VSI. The same analysis can be done for a three-level VSI, and each inverter leg in Fig. 2.5. can be represented as a single-pole-triple-throw switch. The function of this switch can be equivalently represented by three switches Sap, Sao, and San, which are defined as

$$Sap = \begin{cases} 1, & \text{if } S_1 \text{ and } S_{22} \text{ are on} \\ 0, & \text{otherwise} \end{cases},$$

$$Sao = \begin{cases} 1, & \text{if } S_{11} \text{ and } S_{22} \text{ are on} \\ 0, & \text{otherwise} \end{cases}, \text{ and} \qquad (2.1)$$

$$San = \begin{cases} 1, & \text{if } S_{11} \text{and } S_2 \text{ are on} \\ 0, & \text{otherwise} \end{cases},$$

where

$$Sap + Sao + San = 1. \qquad (2.2)$$

For example, when S_1 and S_{22} in Fig. 2.5.(a) are on then $Sap = 1$, $Sao = 0$, and $San = 0$. Complete switching function representation of the three-level VSI circuit is given in Fig. 2.6.

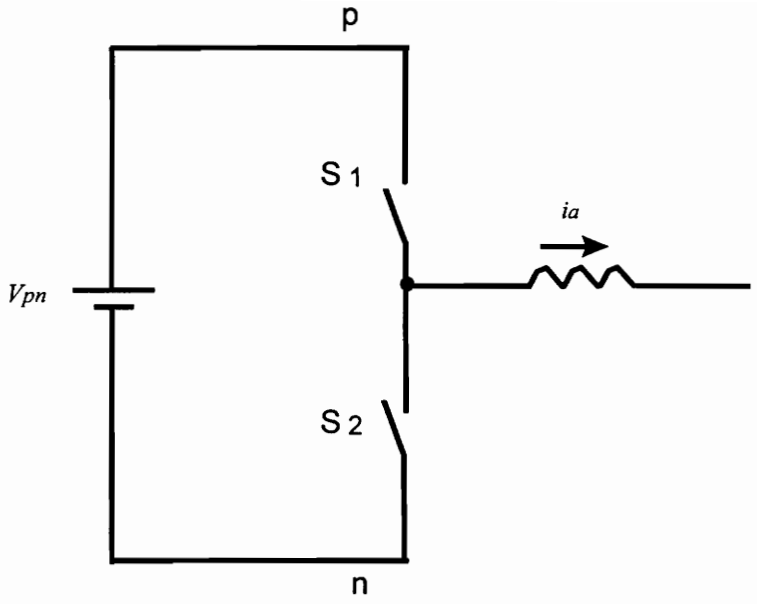

(a) One leg

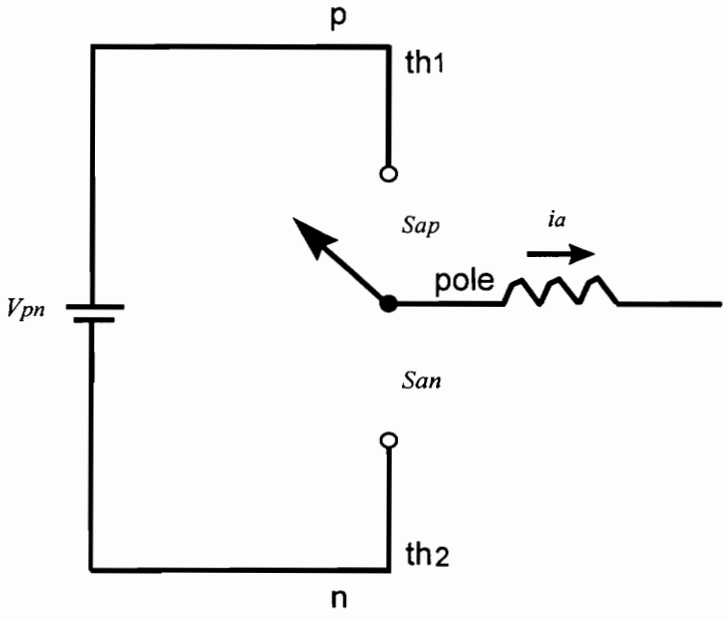

(b) Switching function representation of one leg

Fig. 2.3. A two-level VSI leg represented as two switches.

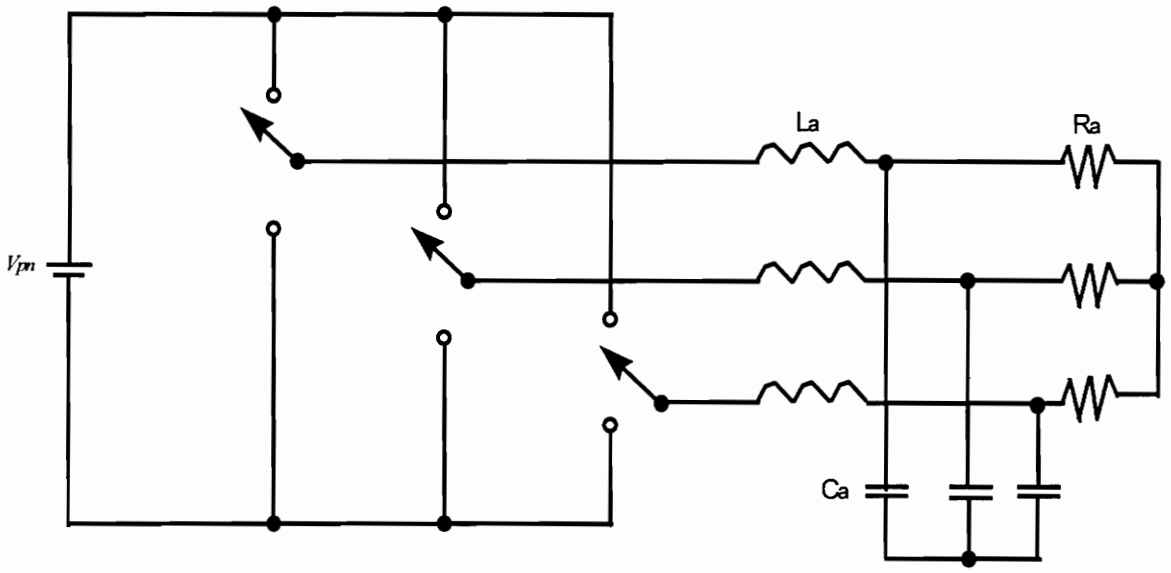

Fig. 2.4. Single-pole-double-throw switch representation of a two-level VSI

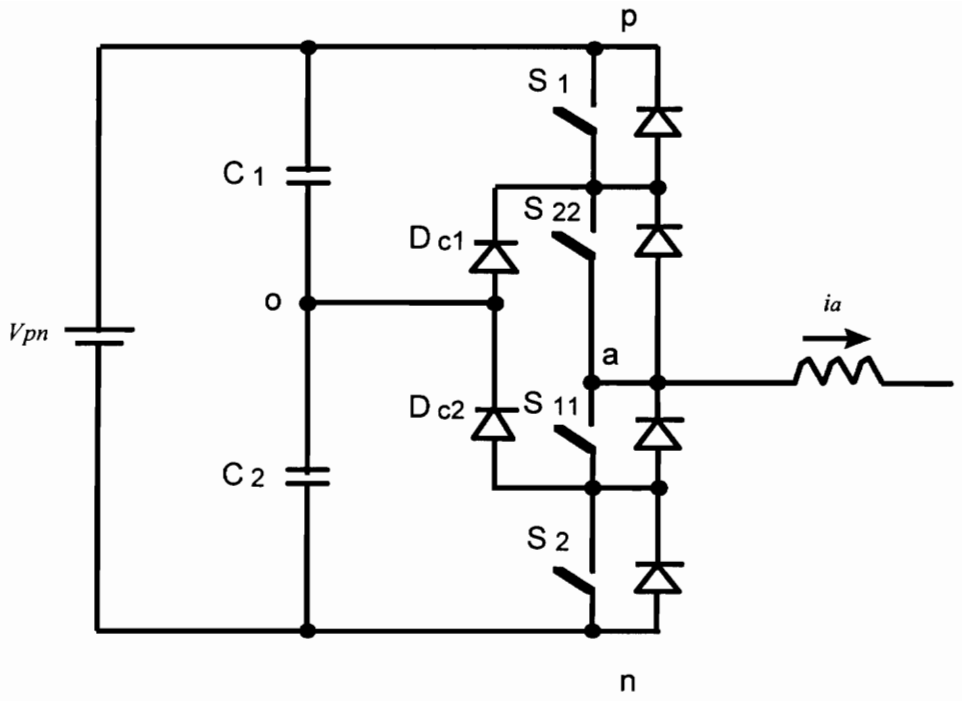

(a) One leg

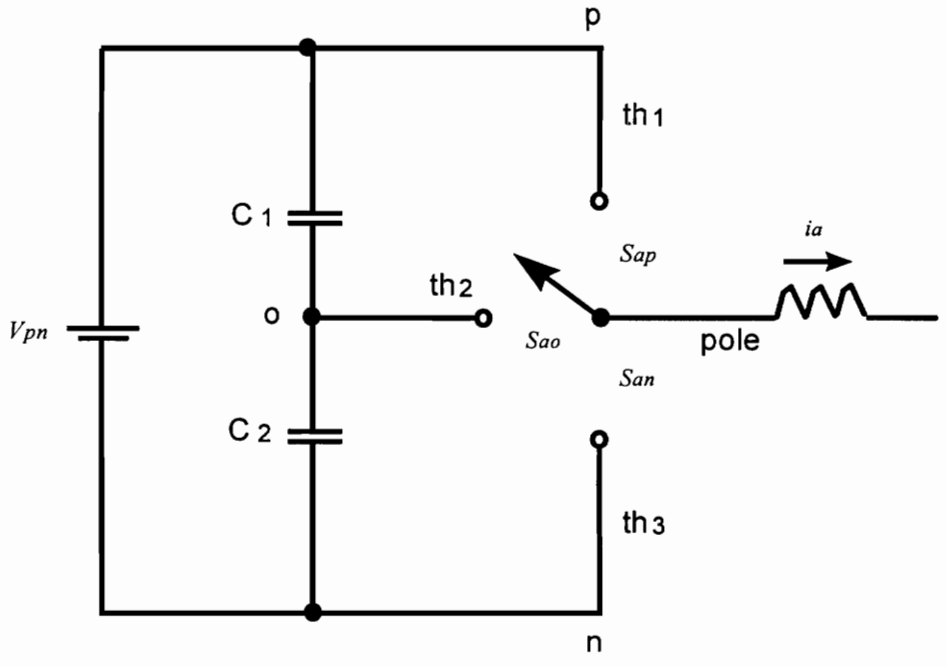

(b)) Switching function representation

Fig. 2.5. A three-level VSI leg represented as three switches.

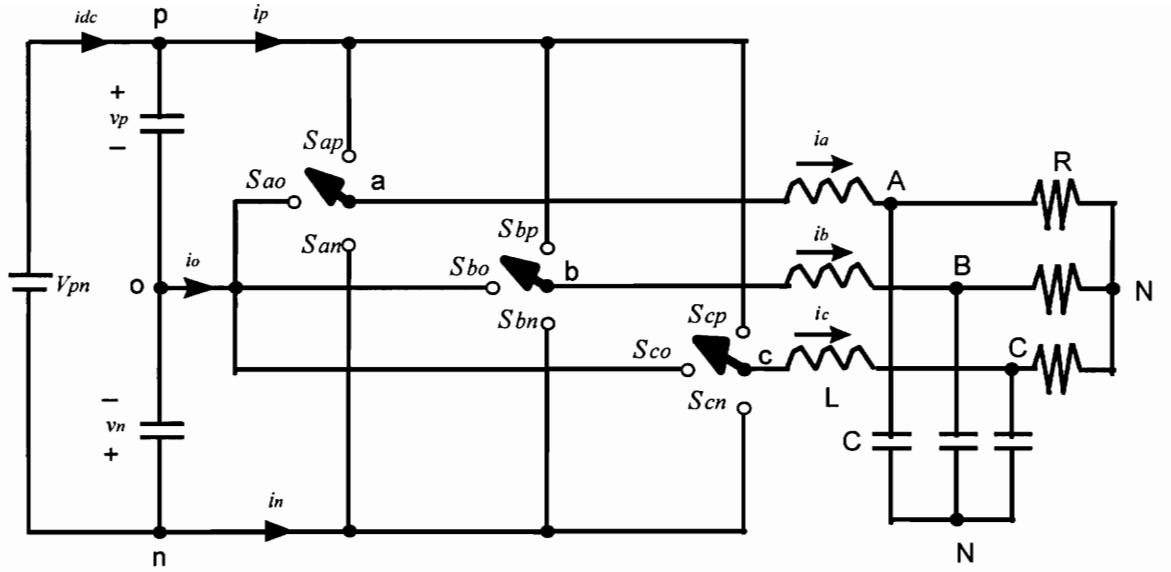

Fig. 2.6. Switching function representation of three-level VSI.

From Fig. 2.6., output line-to-midpoint voltages (vao, vbo, vco) can be written in terms of input voltages (vp, vn), and input currents (ip, in) can be written in terms of output line currents (ia, ib, ic) by using switching functions. Input/output current and voltage relations of the circuit given in Fig. 2.6. can be completely defined as

$$\begin{bmatrix} vao \\ vbo \\ vco \end{bmatrix} = \begin{bmatrix} Sap & San \\ Sbp & Sbn \\ Scp & Scn \end{bmatrix} \cdot \begin{bmatrix} vp \\ vn \end{bmatrix} = [S] \cdot [vg] \quad , \tag{2.3}$$

and

$$\begin{bmatrix} ip \\ in \end{bmatrix} = [S]^T \cdot \begin{bmatrix} ia \\ ib \\ i_c \end{bmatrix} . \tag{2.4}$$

For example, when the poo switching state is applied, above matrix equations can be written as

$$\begin{bmatrix} vao \\ vbo \\ vco \end{bmatrix} = \begin{bmatrix} 1 & 0 \\ 0 & 0 \\ 0 & 0 \end{bmatrix} \cdot \begin{bmatrix} vp \\ vn \end{bmatrix} , \tag{2.5}$$

and

$$\begin{bmatrix} ip \\ in \end{bmatrix} = \begin{bmatrix} 1 & 0 & 0 \\ 0 & 0 & 0 \end{bmatrix} \cdot \begin{bmatrix} ia \\ ib \\ i_c \end{bmatrix} . \tag{2.6}$$

Note that, midpoint current is

$$io = -ip - in . \tag{2.7}$$

2.3 Space Vector Representation of Three-Level VSI Voltages

Space vector representation is a very useful and common method of analyzing three-phase converter circuits [9]. As an example, switching states poo and onn can be shown in a complex plane as in Fig. 2.7., so that the projections of vector **V01** on line-to-line voltage axes are $vab = {}^{Vpn}/_{2}$, $vca = 0$, and $vca = {}^{-Vpn}/_{2}$. This requires the magnitude of vector **V01** to be ${}^{Vpn}/_{\sqrt{3}}$ and the angle to be 0°. Switching states shown in Table 2 have magnitude and phase information that can be expressed in terms of voltage space vectors as in Fig. 2.8. The switching vectors of the three-level VSI can be divided into four groups according to their magnitudes: zero vectors, small vectors, **V01**, ..., **V06** , medium vectors, **V12**, ...**V61**, and large vectors, **V1**, ..., **V6**. Different switching vectors have different effects on the charge balance of the midpoint, output ripple, and switching loss. Each small vector represents two different switching combination, positive and negative. For example, vector **V01**, when it is obtained from the combinations poo is called a positive-combination-vector (**V01p**), and when it is obtained from noo, it is called negative-combination-vector (**V01n**). Both vectors produce the same output voltage, but when the positive vectors are applied, the upper capacitor is charged or discharged, and when the negative vectors are applied, the lower capacitor is charged or discharged. This property of the small vectors provides the freedom which can be used to control the charge balance of the dc-link midpoint. Combinations that produce medium vectors also affect the midpoint voltage, but there is only one combination for each vector. Lastly, large vectors and zero vectors do not change the voltage of the midpoint. In terms of line-to-line voltages, the magnitude of the large vectors is ${}^{2 \cdot V_{pn}}/_{\sqrt{3}}$, and the magnitude of small vectors is ${}^{V_{pn}}/_{\sqrt{3}}$. The magnitude of the medium vector is equal to V_{pn}, which is the same as the maximum radius of a

circle that can be inscribed into the large hexagon in Fig. 2.8. Therefore, the maximum amplitude of undistorted output line voltage is V_{pn}.

The desired output line voltage vector in steady-state can be represented as:

$$\mathrm{V}(\theta) = D\mathrm{mod} \cdot Vpn \cdot e^{j(\theta - 30^{o})}, \qquad \theta = \omega \cdot t \tag{2.8}$$

where $0 \le |\mathrm{V}| \le Vpn$ is the output line voltage, $0 \le D\mathrm{mod} \le 1$ is the modulation index, and ω is the frequency of the output voltage. From the modulation index ($D\mathrm{mod}$) a parameter dm is defined as $dm = \frac{\sqrt{3}}{2} \cdot D\mathrm{mod}$, where $0 \le dm \le \frac{\sqrt{3}}{2}$.

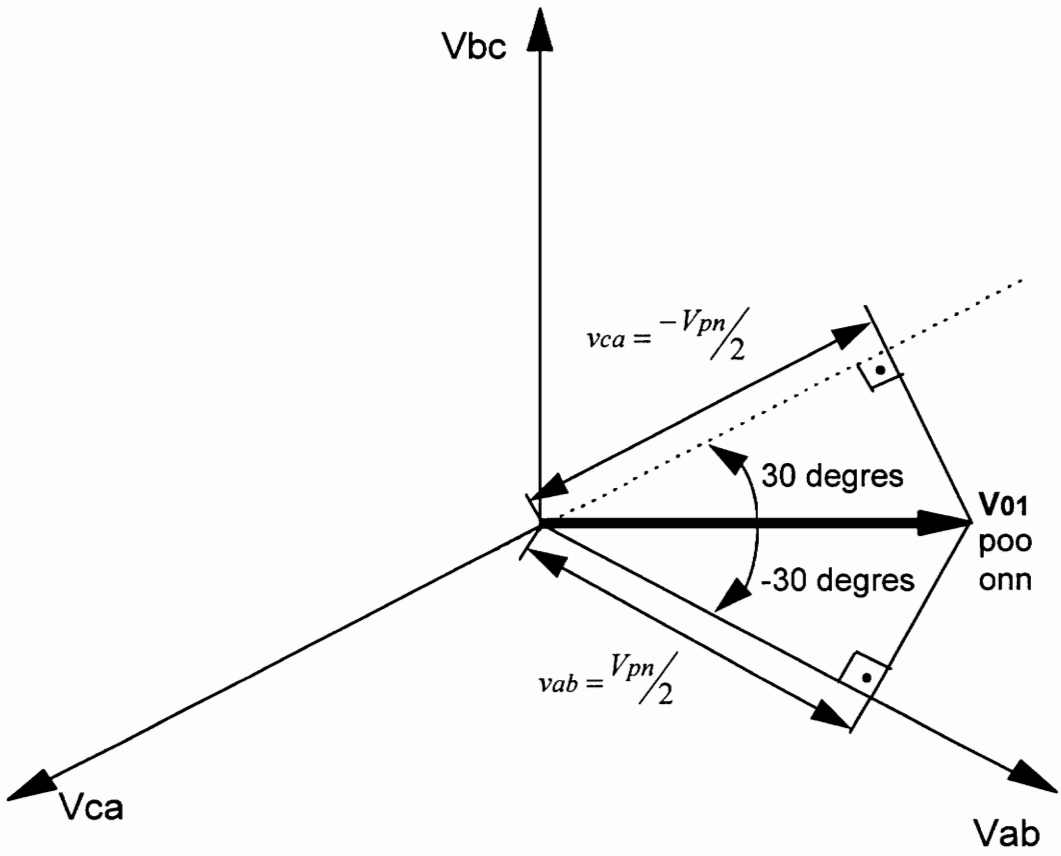

Fig. 2.7. Representing switching states poo and onn in space vector form.

Table 2 Switching states in a three-level VSI and corresponding outputs

Switching states	Name of the vector	vab	vbc	vca	io	ip
ppp	**V0**	0	0	0	0	0
nnn	**V0**	0	0	0	0	0
ooo	**V0**	0	0	0	0	0
poo	**V01p**	Vpn/2	0	-Vpn/2	$ib+ic$	ia
onn	**V01n**	Vpn/2	0	-Vpn/2	ia	0
ppo	**V02p**	0	Vpn/2	-Vpn/2	ic	$ia+ib$
oon	**V02n**	0	Vpn/2	-Vpn/2	$ia+ib$	0
opo	**V03p**	-Vpn/2	Vpn/2	0	$ia+ic$	ib
non	**V03n**	-Vpn/2	Vpn/2	0	ib	0
opp	**V04p**	-Vpn/2	0	Vpn/2	ia	$ib+ic$
noo	**V04n**	-Vpn/2	0	Vpn/2	$ib+ic$	0
oop	**V05p**	0	-Vpn/2	Vpn/2	$ia+ib$	ic
nno	**V05n**	0	-Vpn/2	Vpn/2	ic	0
pop	**V06p**	Vpn/2	-Vpn/2	0	ib	$ia+ic$
ono	**V06n**	Vpn/2	-Vpn/2	0	$ia+ic$	0
pon	**V12**	Vpn/2	Vpn/2	-Vpn	ib	ia
opn	**V23**	-Vpn/2	Vpn	-Vpn/2	0	ib
npo	**V34**	-Vpn	Vpn/2	Vpn/2	ic	ib
nop	**V45**	-Vpn/2	-Vpn/2	Vpn	ib	ic
onp	**V56**	Vpn/2	-Vpn	Vpn/2	ia	ic
pno	**V61**	Vpn	-Vpn/2	-Vpn/2	ic	ia
pnn	**V1**	Vpn	0	-Vpn	0	ia
ppn	**V2**	0	Vpn	-Vpn	0	$ia+ib$
npn	**V3**	-Vpn	Vpn	0	0	ib
npp	**V4**	-Vpn	0	Vpn	0	$ib+ic$
nnp	**V5**	0	-Vpn	Vpn	0	ic
pnp	**V6**	Vpn	-Vpn	0	0	$ia+ic$

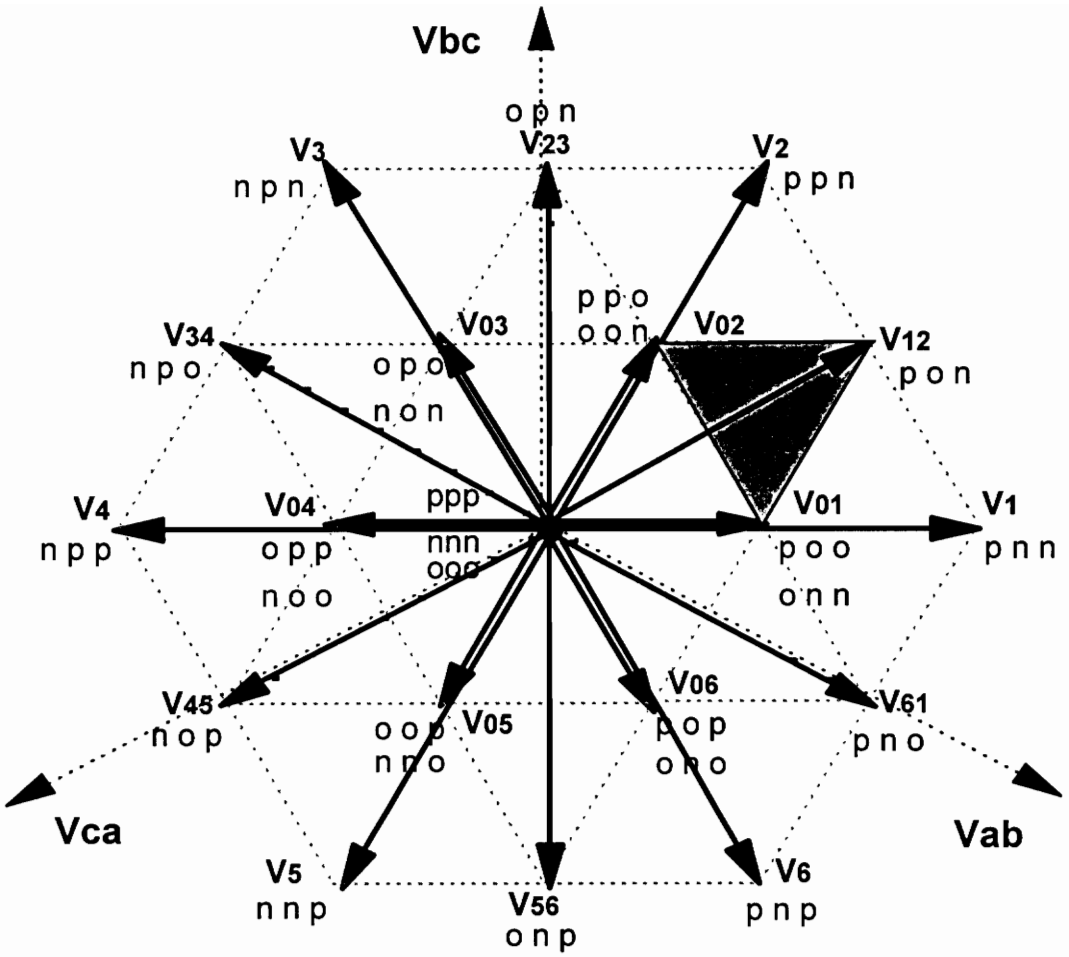

Fig. 2.8. Space vector representation of three-level VSI line voltages.

2.4 Space Vector Modulation

The principle of SVM is to approximate the reference vector **V** in (2.8), over one switching period, by using PWM of switching vectors in Fig. 2.8. The task can be divided into two parts: first, selection of the switching vectors to be used, and second, calculating the duty cycles of the selected vectors. Due to the large number of switching vectors, there is a freedom in the choice of the vectors and their duty cycles. This freedom can be used to optimize the following goals:

- minimum harmonics in the output waveforms,
- minimum midpoint current i_o,
- minimum number of switching actions (i.e. minimum switching losses).

The output voltage harmonics can be minimized (resulting in a small ripple of the output current) if only the switching vectors nearest to the reference vectors are selected for PWM. This is achieved by using adjacent switching vectors located at the corners of the small triangle in which the reference vector is located at a given instant. 24 small equilateral triangles within the hexagon can be identified in Fig. 2.8., and the location of the reference vector can be found from the geometry.

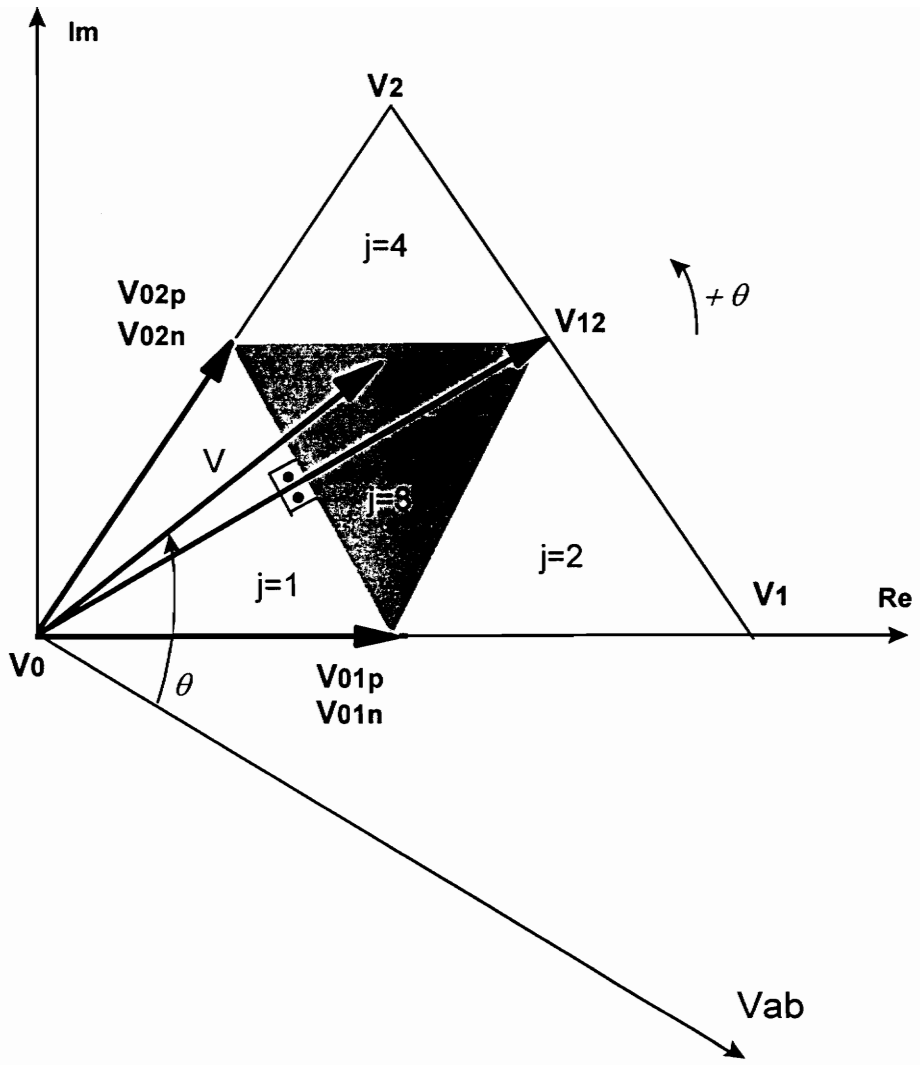

Fig. 2.9. One of the sixty degree intervals in Fig. 2.8.

Due to the circular symmetry, operation and duty cycle calculations can be explained by using only one of the large triangles, Fig. 2.9. For the shaded small triangle in Fig 2.9., the vector summation equations can be written as

$$\begin{aligned} &\mathbf{V01}\cdot t_{01}+\mathbf{V02}\cdot t_{02}+\mathbf{V12}\cdot t_{12}=\mathbf{V}\cdot T_s \\ &t_{01}+t_{02}+t_{12}=T_s, \end{aligned} \tag{2.9}$$

where t_{01}, t_{02}, t_{12} and are the time duration of the vectors **V01**, **V02**, and **V12**, respectively. Substituting

$$\mathbf{V01}=\frac{Vpn}{\sqrt{3}},\ \mathbf{V02}=\frac{Vpn}{\sqrt{3}}\cdot e^{j\frac{\pi}{3}},\ \mathbf{V12}=Vpn\cdot e^{j\frac{\pi}{6}},\ \text{and}\ \mathbf{V}=D\,\mathrm{mod}\cdot Vpn\cdot e^{j(\theta-\frac{\pi}{6})}$$

and (2.8) into (2.9), t_{01}, t_{02}, $and\ t_{03}$ can be solved as

$$\begin{aligned} t_{01} &= T_s(1-\frac{4}{\sqrt{3}}\cdot dm\cdot\sin(\theta-\frac{\pi}{6})), \\ t_{02} &= T_s(\frac{2}{\sqrt{3}}\cdot dm\cdot\sin(\theta-\frac{\pi}{6})-2\cdot dm\cdot\cos(\theta-\frac{\pi}{6})+1),\ \text{and} \\ t_{12} &= T_s(\frac{2}{\sqrt{3}}\cdot dm\cdot\sin(\theta-\frac{\pi}{6})+2\cdot dm\cdot\cos(\theta-\frac{\pi}{6})-1), \end{aligned} \tag{2.10.a}$$

where $dm=D\,\mathrm{mod}\cdot\frac{\sqrt{3}}{2}$. From (2.10.a), duty cycles for the vectors **V01**, **V02**, and **V12** can be defined as

$$d01=\frac{t_{01}}{T_s},\ d02=\frac{t_{02}}{T_s},\ \text{and}\ d12=\frac{t_{12}}{T_s}. \tag{2.10.b}$$

In order to minimize the midpoint current, i.e. reduce the charge unbalance of the input capacitors, positive and negative combinations of the small switching vectors can be used alternately within each or alternate switching cycles. An example of ordering the switching vectors is shown in Fig. 2.10. and Fig. 2.11. In this example, oon and onn switching states utilize the lower dc-link capacitor while poo switching state utilizes the upper dc-link capacitor. On the

other hand, pon switching state utilizes the upper and lower dc-link capacitors but the ratio of the upper and lower dc-link capacitor currents depends on the instantaneous value of the load current.

When **V01** vector is split into two equal pieces, it has no effect on the midpoint voltage. **V02n** and **V12** vectors may have good or bad effects on the midpoint voltage, depending on the instantaneous value of the load current, which is not investigated in this work. The same way, **V02** vector can be split into two pieces as **V02p** and **V02n** in one switching cycle. In this case, **V02** has no effect on the midpoint voltage, but the effect of the **V01n** and **V12** may be good or bad, depending on the instantaneous value of the load current.

In Fig. 2.10, after **V01p** is applied, only one switching action is required to apply the next vector **V12**. For the next switching cycle, the reverse order of the above shown vectors can be applied to minimize the switching action and output ripple. Table 3 shows the order of the vectors to apply for the big triangle in Fig. 2.9.

Duty cycle calculations for other triangles can be done in a similar way for other small triangles in Fig. 2.9. Appendixes A and B show the sequence of the vectors used in every triangle and duty cycle calculations.

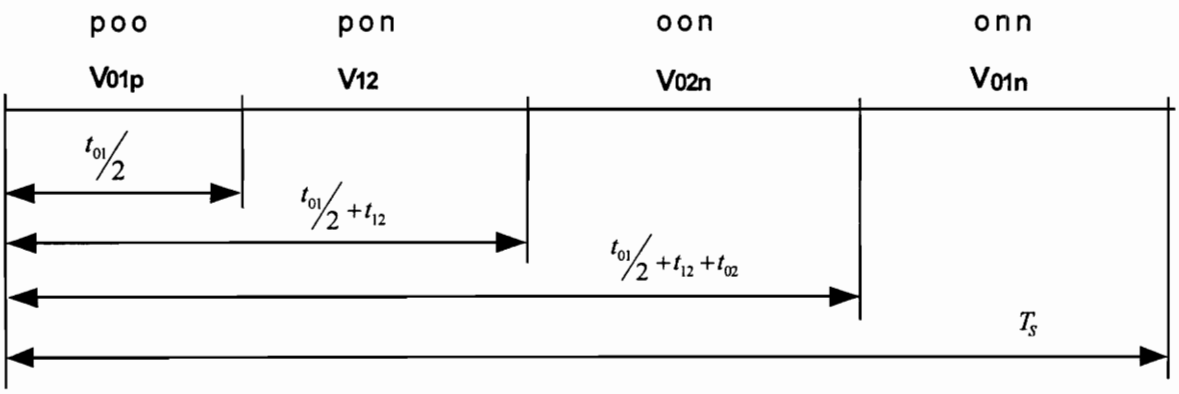

Fig. 2.10. Sequence of the vectors in one cycle.

For the next switching cycle, above vectors are applied in reverse order.

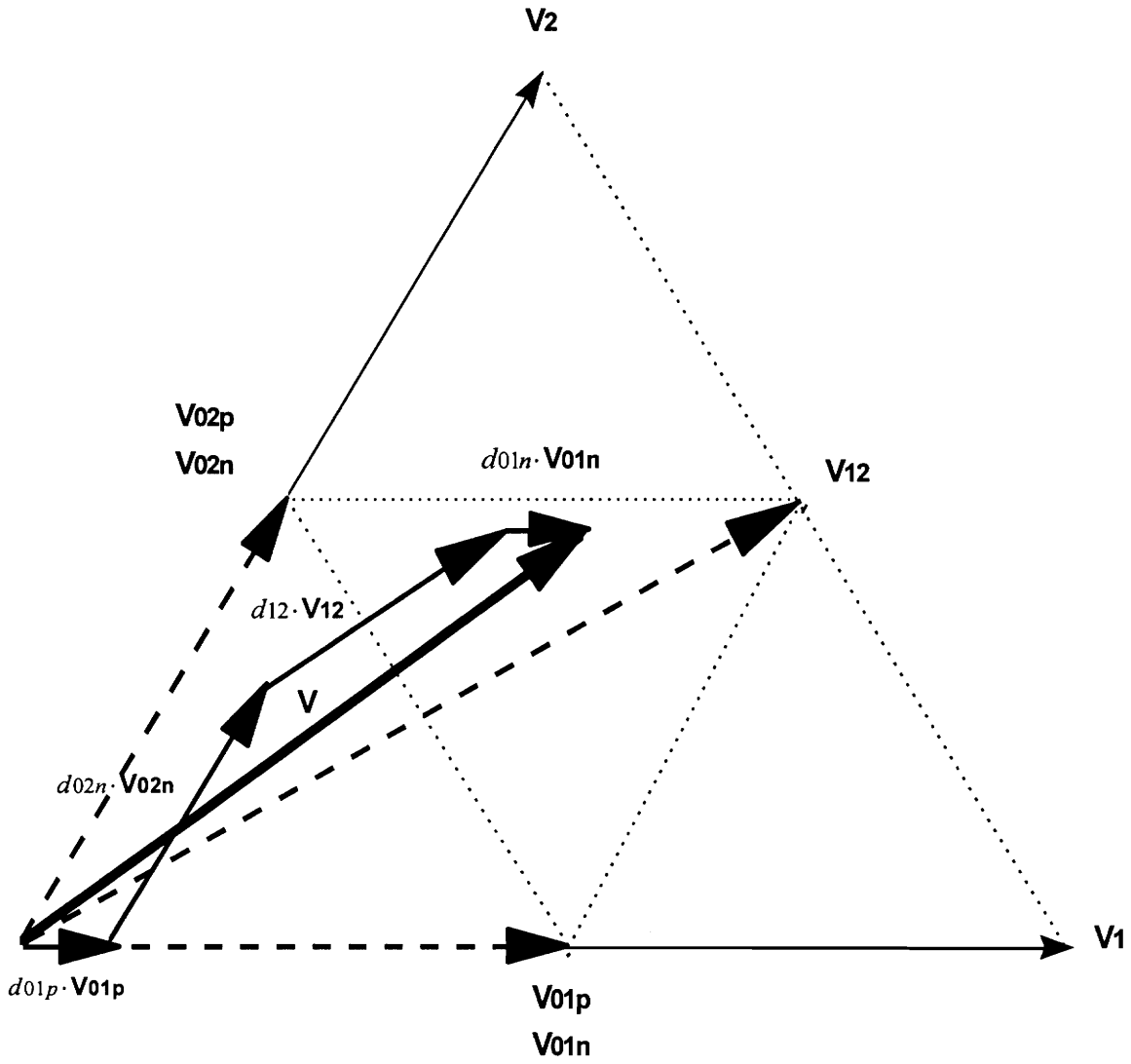

Fig. 2.11. Synthesis of the reference vector "v"

Table 3 The sequence of the switching vectors in first sixty degree interval

Index of the triangles in Fig 2.9.	Vector sequence
j=1	**V_{01p}, V_0, V_{02n}, V_{01n}**
j=2	**V_{01p}, V_{12}, V_1, V_{01n}**
j=3	**V_{01p}, V_{12}, V_{02n}, V_{01n}**
j=4	**V_{02p}, V_2, V_{12}, V_{02n}**

3. SIMULATION OF THREE-LEVEL VSIs

3.1. Simulation Program

In many industry applications, prior to building large electrical and electromechanical systems, a simplified model is developed and investigated by simulation. It provides better understanding of the system and allows to evaluate different control algorithms easily. This process reduces the time and money needed to develop the prototype of the converter.

A SABER simulation program is developed for time domain simulation of three-level three-phase inverter system. SABER is a powerful and widely used simulation program introduced by Analogy Inc.

Fig. 3.1. shows the block diagram of the simulation circuit. There are two input files, one is the main file to create netlist which is for the three-level VSI. The second file is the SVM file and it performs the SVM algorithm to drive the switches in main file.

Main file is the netlist of the power stage and is relatively strait forward. As simulation time is swept from zero to desired value, main file runs the SVM file to find the duty cycles and to derive the switches. Switches in power circuit are considered as ideal to make the simulation simple. Resistors are used as three phase load. For a nonresistive load, the phase between the voltage and current should be taken into account in the SVM algorithm.

SVM file is a text file written in MAST which is the modeling language for the Saber simulator. All electrical and electromechanical device models in Saber library are written in MAST language. These files are called “templates”. MAST models all elements by their characteristic equations. Saber provides the library for commonly used components. However, there is no Space Vector Modulation template in Saber. That is why, developing a MAST file to implement the SVM algorithm for three-phase three-level VSI is a requirement for time domain simulation.

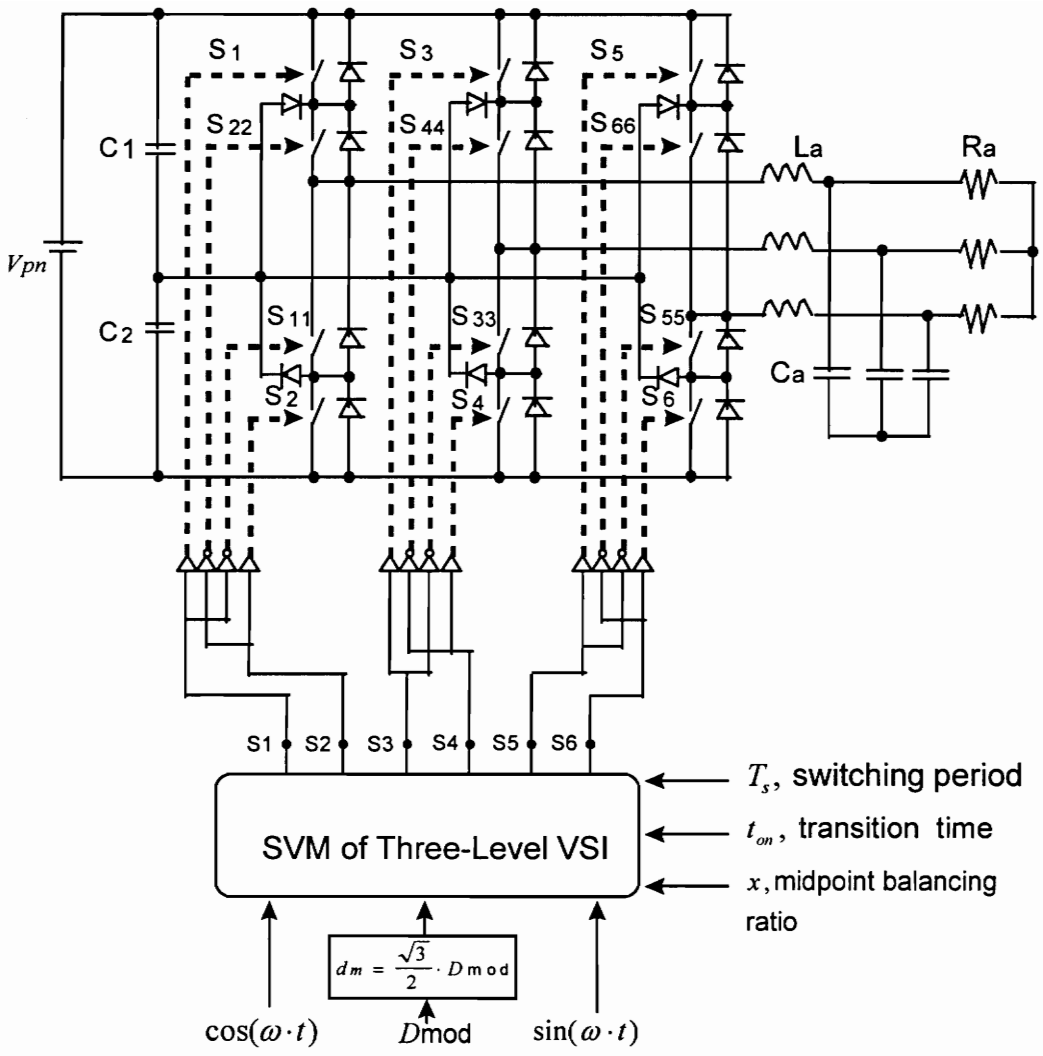

Fig. 3.1. Block diagram of the Saber simulation

3.2. Space Vector Modulator

The purpose of the SVM algorithm is to determine the small triangle in which the reference vector is located at a given instant and to find the duty cycles of each switching vector forming that particular triangle.

Depending on the application, the reference output voltage vector may be obtained in several different forms, such as three described output line voltages $(vab(t),\ vbc(t), vca(t))$, or as their two-phase transformation in stationary or rotating coordinate systems [10] or in complex form as in (2.8). In our simulation algorithm we assumed a two-phase representation in stationary coordinates. From (2.8), we can define

$$dref = \frac{\mathbf{V}}{\frac{2}{\sqrt{3}} \cdot Vpn} = \frac{\sqrt{3}}{2} \cdot D \bmod \cdot e^{j\cdot(\theta - \frac{\pi}{6})} \tag{3.1}$$

as "reference duty-cycle vector". Also, all voltage vectors in the space vector hexagon in Fig. 2.8 and 2.11 can be divided by $\frac{2}{\sqrt{3}} \cdot Vpn$ to obtain a duty-cycle space vector hexagon. One 60° sector of this hexagon is shown in Fig. 3.2, together with the reference vector (3.1).

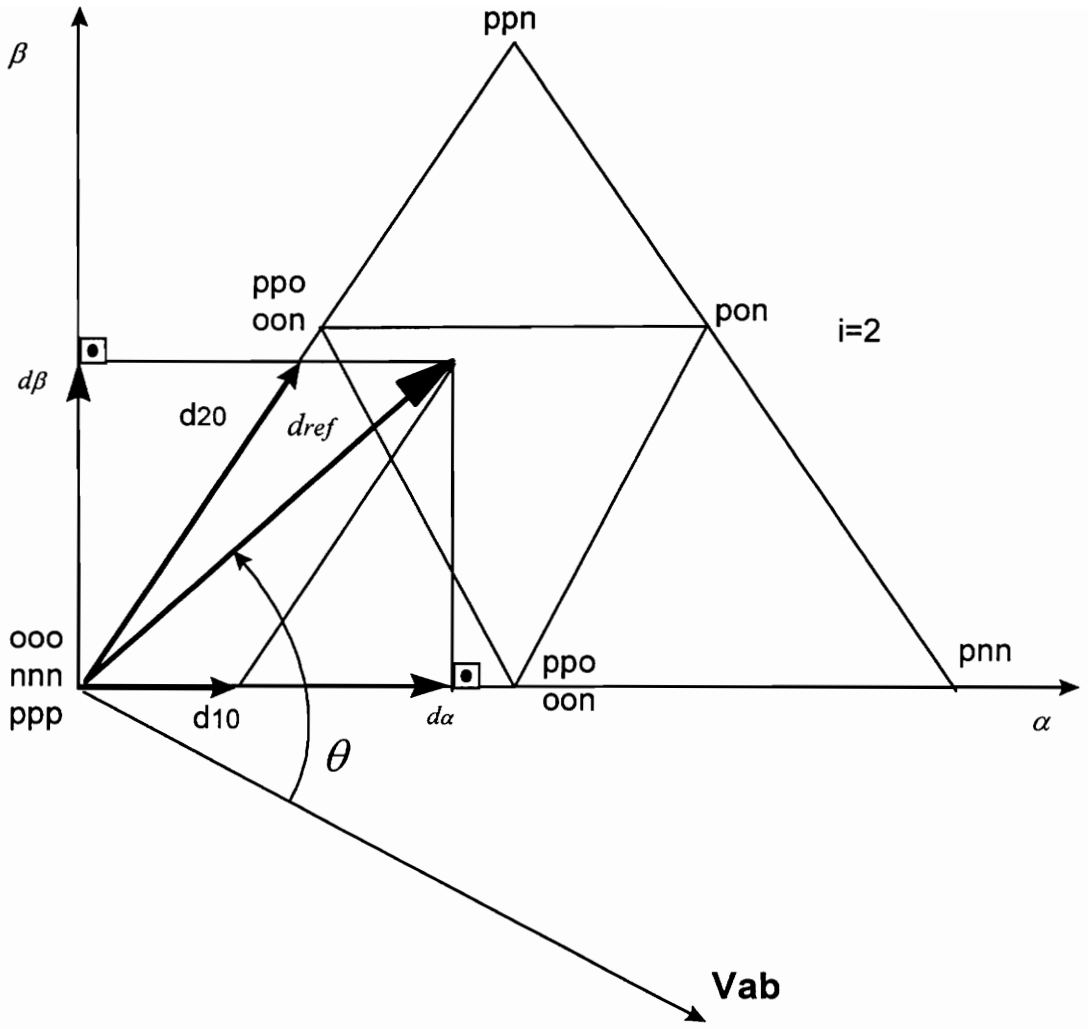

Fig. 3.2. Finding the $d\alpha$ and $d\beta$ projections

From the geometry in Fig. 3.2., the projection of the reference vector on α and β axis is written as

$$d\alpha = \frac{\sqrt{3}}{2} \cdot D\,\mathrm{mod} \cdot \cos(\theta - 30^o), \text{ and}$$
$$d\beta = \frac{\sqrt{3}}{2} \cdot D\,\mathrm{mod} \cdot \sin(\theta - 30^o) \tag{3.2}$$

where

$$\theta = \omega \cdot t\ . \tag{3.3}$$

In Equation 3.2, $D\,\mathrm{mod}$ is the modulation index and ω is the frequency of the output voltage. In addition to $d\alpha$ and $d\beta$ parameters, the followings are the other inputs of the algorithm:

T_s	the switching period
TT	two times of the switching period
ton	very small transition time
$D\,\mathrm{mod}$	modulation index, $0 \le D\,\mathrm{mod} \le 1$
x	the parameter that divides the small vectors into

two pieces. For example, if the duty cycle of the small vector is $d01$ then, $d01p = x \cdot d01$, and $d01n = (1 - x) \cdot d01$ which are the duty cycles of the positive and negative small vectors.

In Fig. 3.3., $d10$ and $d20$ represents the projection of the reference vector on the apexes of the large equilateral triangle. This duty cycles are used to determine the small equilateral triangle where the reference vector is located and to find the duty cycles of the space vectors which form the small equilateral triangles.

Space Vector Modulation algorithm, first of all, finds the location of the reference vector in the large hexagon, i.e. determination of the "i" parameter, where i=1,2,...,6. This is done by comparing the sign of the alpha and beta projections. For example, for i=2 sixty degree interval, $d\alpha \cdot d\beta > 0$ and $d\beta > 0$. The other sixty degree intervals are determined the same way.

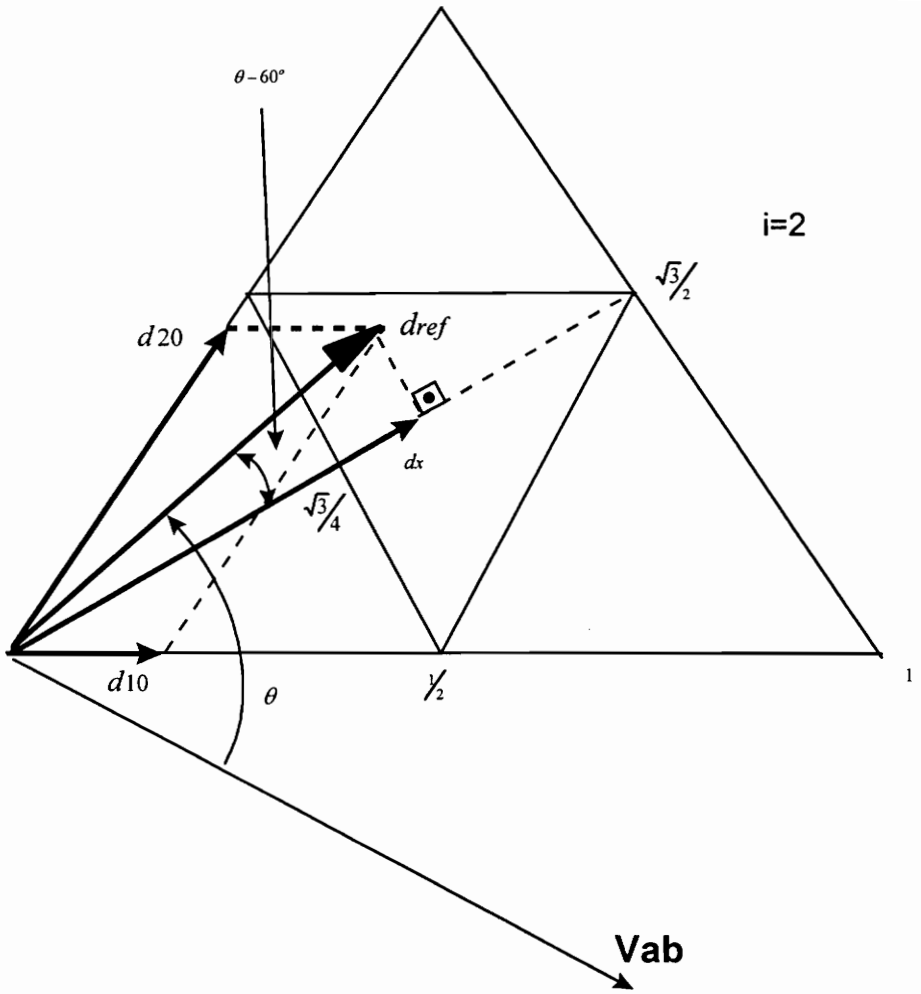

Fig. 3.3. Finding dx

Second, to determine in which small triangle the reference vector is, i.e. to find the "j" parameter, where j=1,2,3,4, we need to find the $d10$ and $d20$ duty cycles. Then there are four options:

1) If $d10$ is larger than 0.5 then the reference vector is located in j=1 triangle. Then duty cycles for the vectors forming this triangle are calculated as in Appendix B.

2) If $d20$ is larger than 0.5 then the reference vector is located in j=3 triangle, and then duty cycles are calculated the same way.

3) If 1 and 2 or nor true, then reference vector is located in j=2 or j=1. In this point an other parameter is necessary to define, i.e. dx. The parameter dx is the projection of the reference vector on the axis where the medium vectors are located. For i=2 sixty degree interval,

$$dx = \frac{\sqrt{3}}{2} \cdot D \bmod \cdot \cos(\theta - 60^o) \qquad (3.4)$$

and since cosine is an even function whether θ is less or bigger than 30° does not make and difference. Then, if dx is larger than $\sqrt{3}/4$, the reference vector is located in j=2 triangle, if not, then it is located in j=4 triangle. The parameter dx can be calculated the same way for other sixty degree intervals.

Fig. 3.4. shows all 24 small equilateral triangles. Above explained algorithm finds the i,j combination for a given reference vector which can be anywhere inside the large hexagon.

The complete SVM algorithm as a flow chart is given in Appendix D.

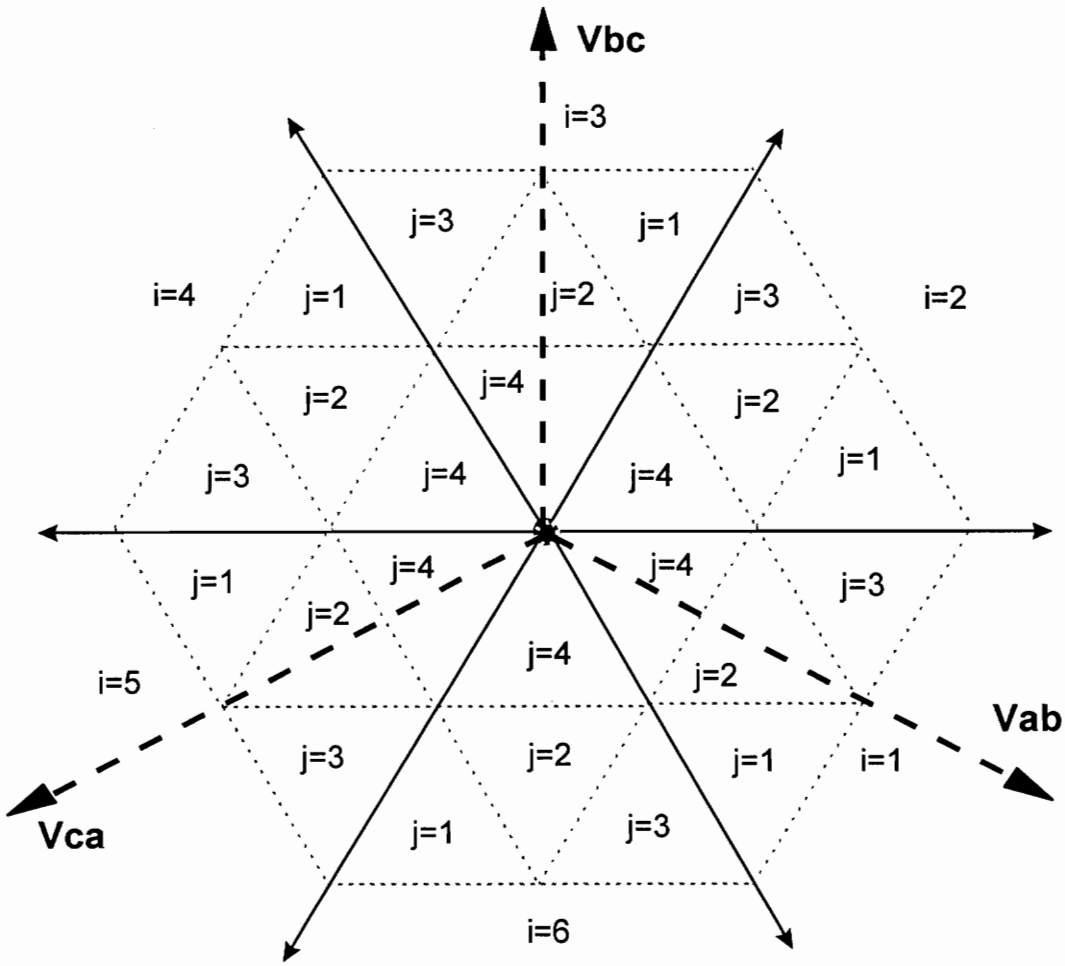

Fig. 3.4. Each small equilateral triangle is represented by i,j combinations

3.3. Simulation Results

Saber simulation of a 250 kW three-phase three-level VSI is performed to test the SVM algorithm, to observe if the voltage across the input capacitors are constant at half of the DC bus voltage, and to determine the inductor which gives 20 % current ripple. The most important reason of simulation is to test the SVM algorithm. The same algorithm can be easily implemented on a DSP board for a prototype circuit. Fig. 3.5. shows the circuit parameters used to get the time domain results. Output line frequency is chosen as 60 Hz. One cycle simulation of three-phase three-level VSI on a Sun Sparc Station 10 takes about 3 hours. The following voltages and currents in Fig. 3.5. are chosen as simulation outputs.

Output line currents (ia , ib , ic)

Harmonic content of the output currents,

Output line to line voltages (vab , vAB , vBC , vCA), and

Midpoint voltage, -vn.

Fig. 3.6. and 3.7. show the output line currents in one cycle and in a sixty degree interval. It can be seen from the results that, peak line current is 210 A, and peak-to-peak ripple is about 20 %. Sixty degree interval of line currents shows that current crossing is smooth. Line currents cross each other at every sixty degrees where the reference vector moves from one sixty degree interval to an other. SVM algorithm should be good enough to provide a smooth current crossing.

Fig. 3.8. shows the output line-to-line voltages before and after the output filter. Line to line voltage before the output filter is a time discontinuous voltage and has zero, half of the line voltage and full dc-bus voltage in each direction, which is a distinct feature of a three-level VSI. Fig. 3.9. shows the midpoint voltage which is constant at half of the dc-bus voltage but has a third order low frequency swing. This voltage swing is caused by medium vectors. As rotating vector moves close to medium vectors, one of the capacitors are discharged slightly more than the other.

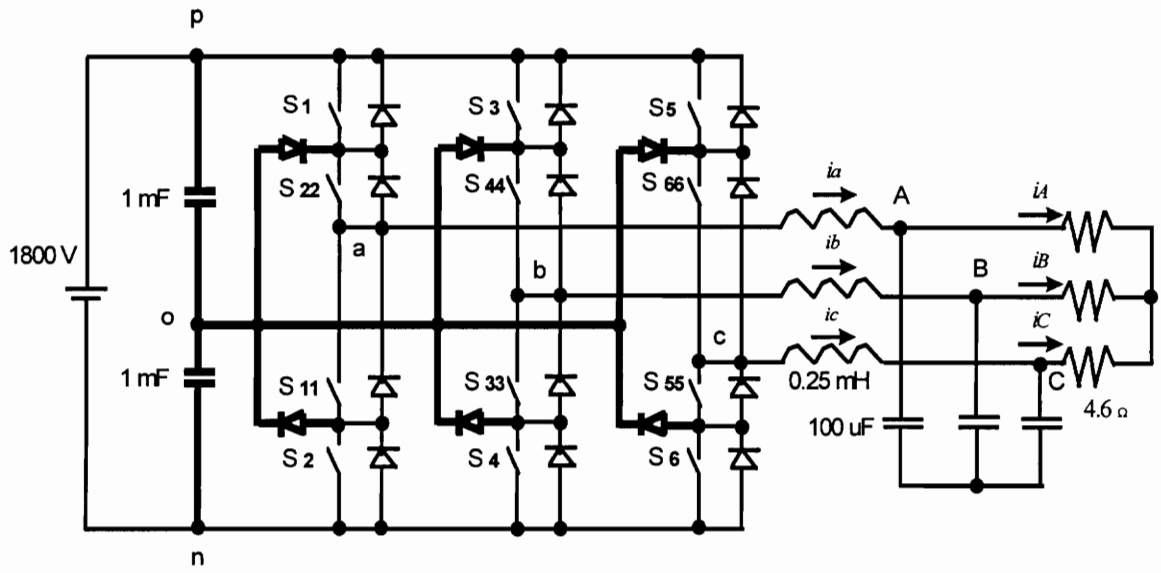

Fig. 3.5. Circuit parameters for Saber simulation

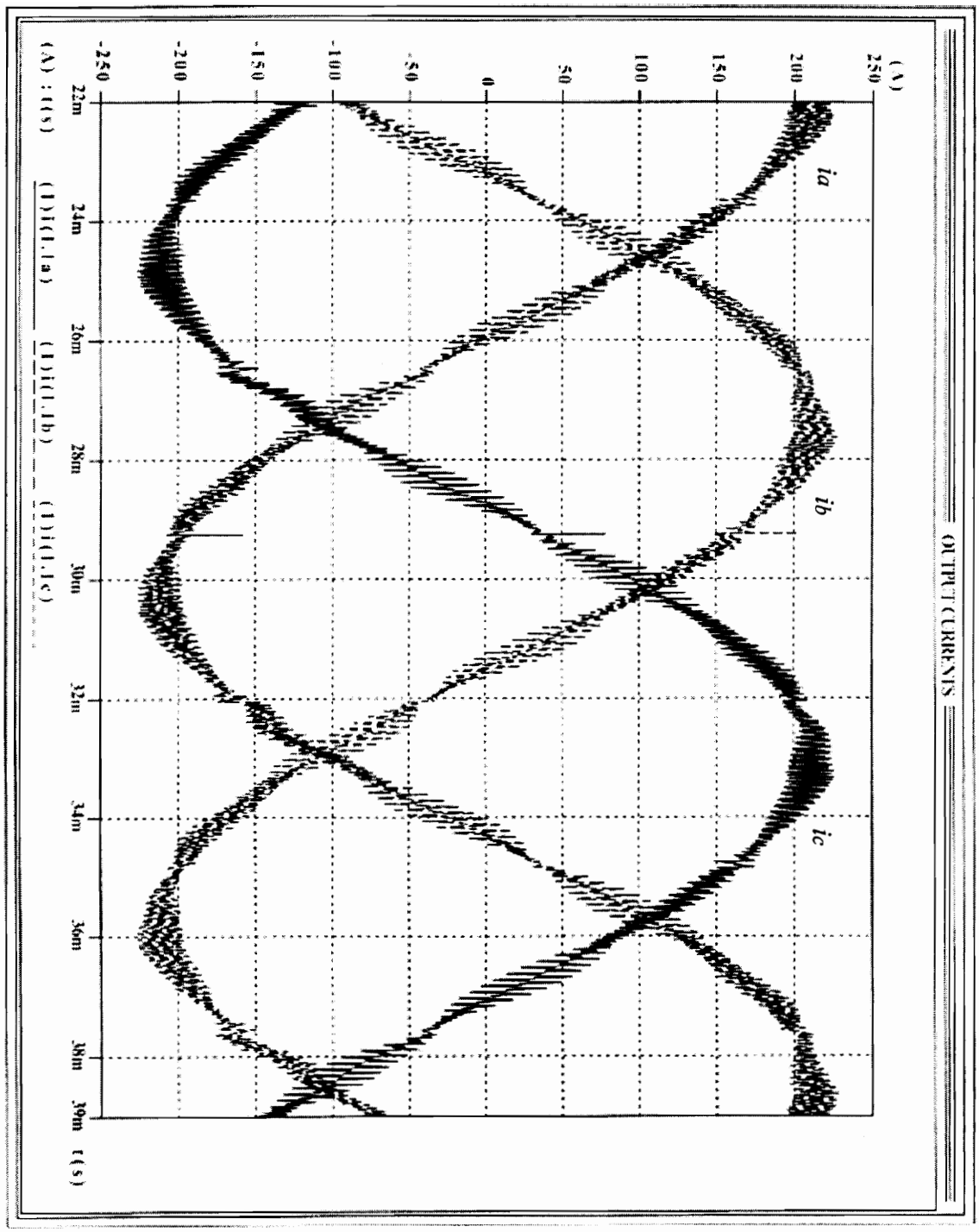

Fig. 3.6. Output line currents, ia, ib, ic

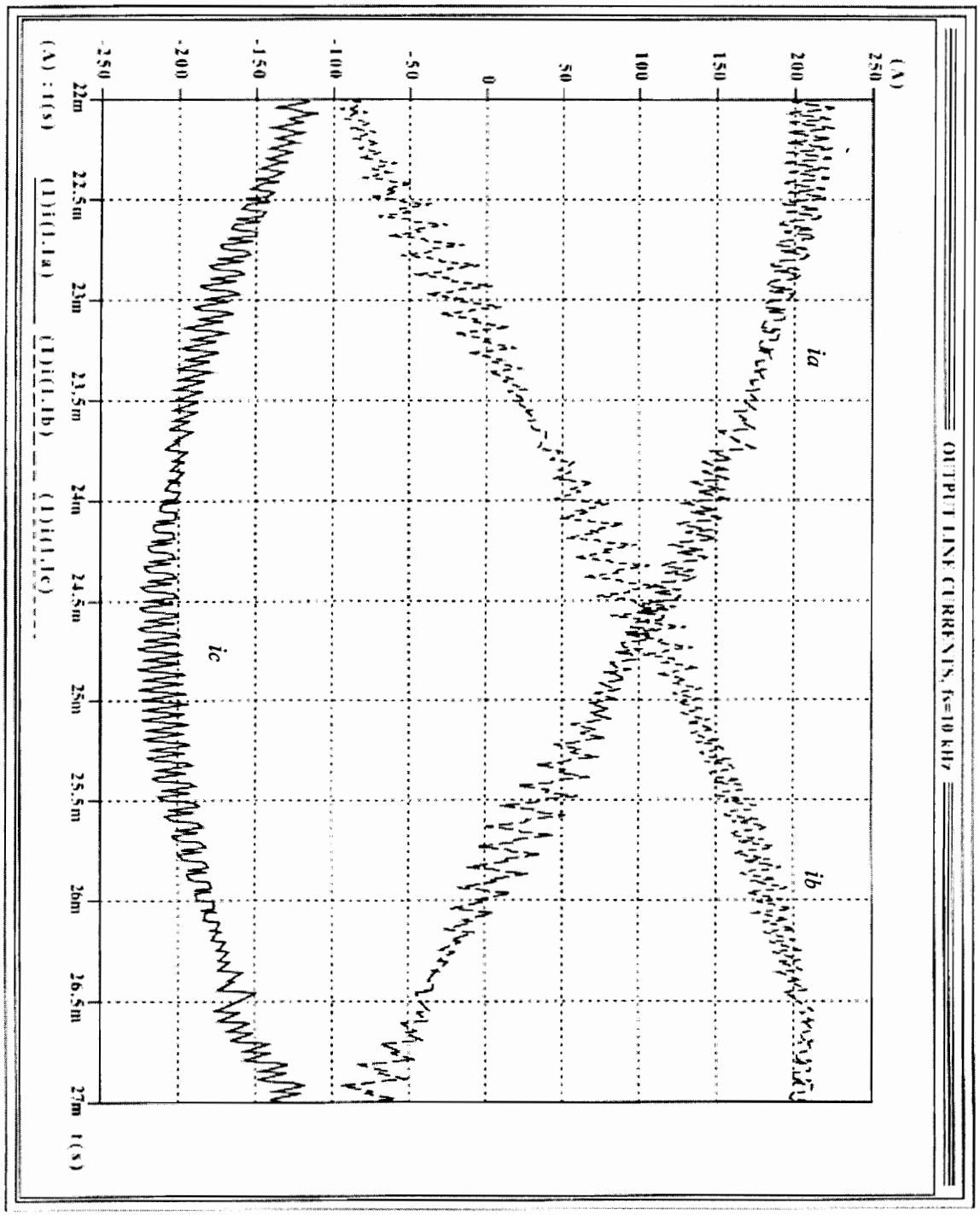

Fig. 3.7. Output line currents in a sixty degree interval

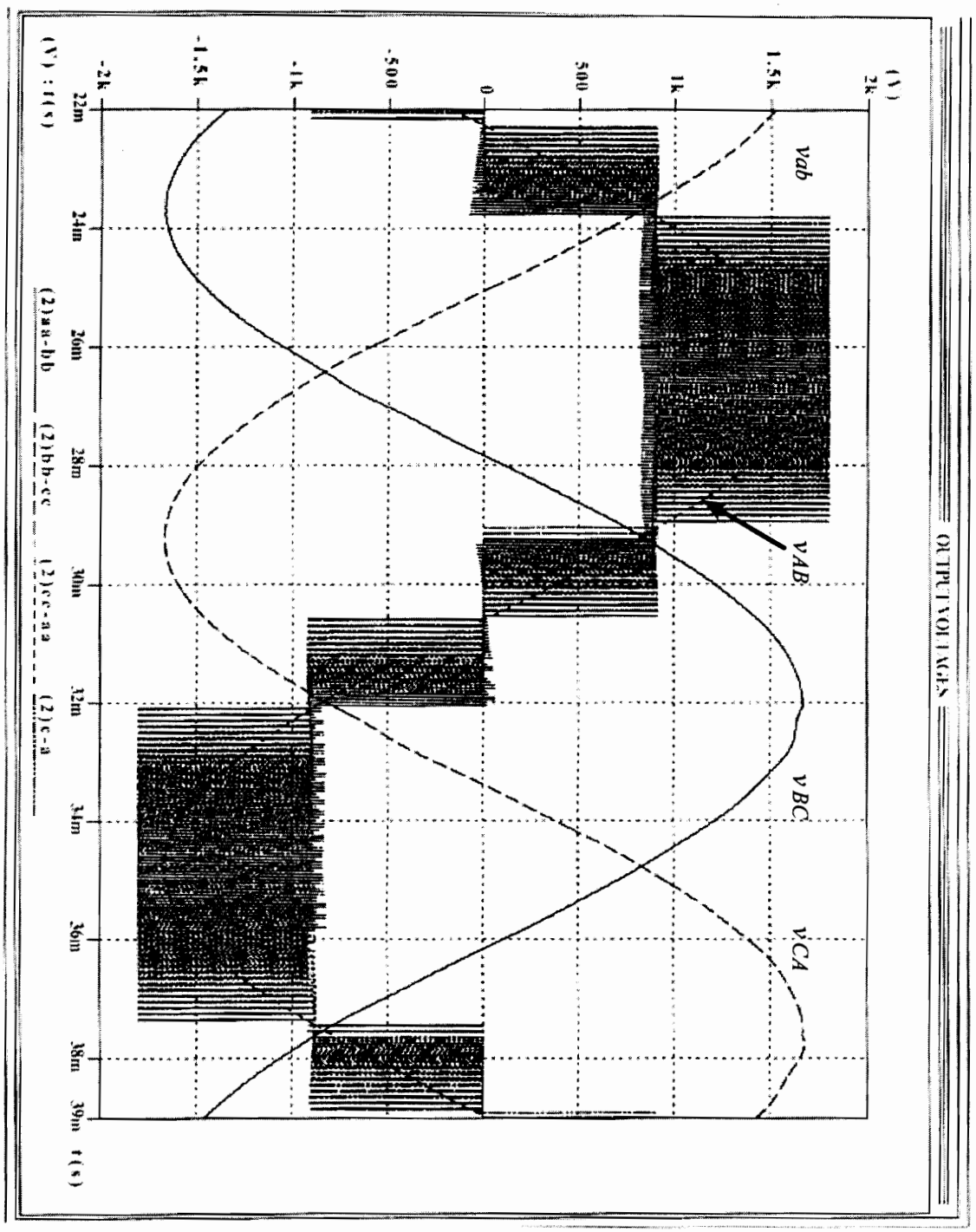

Fig. 3.8. Output line-to-line voltages, v_{ab}, v_{AB}, v_{BC}, and v_{CA}

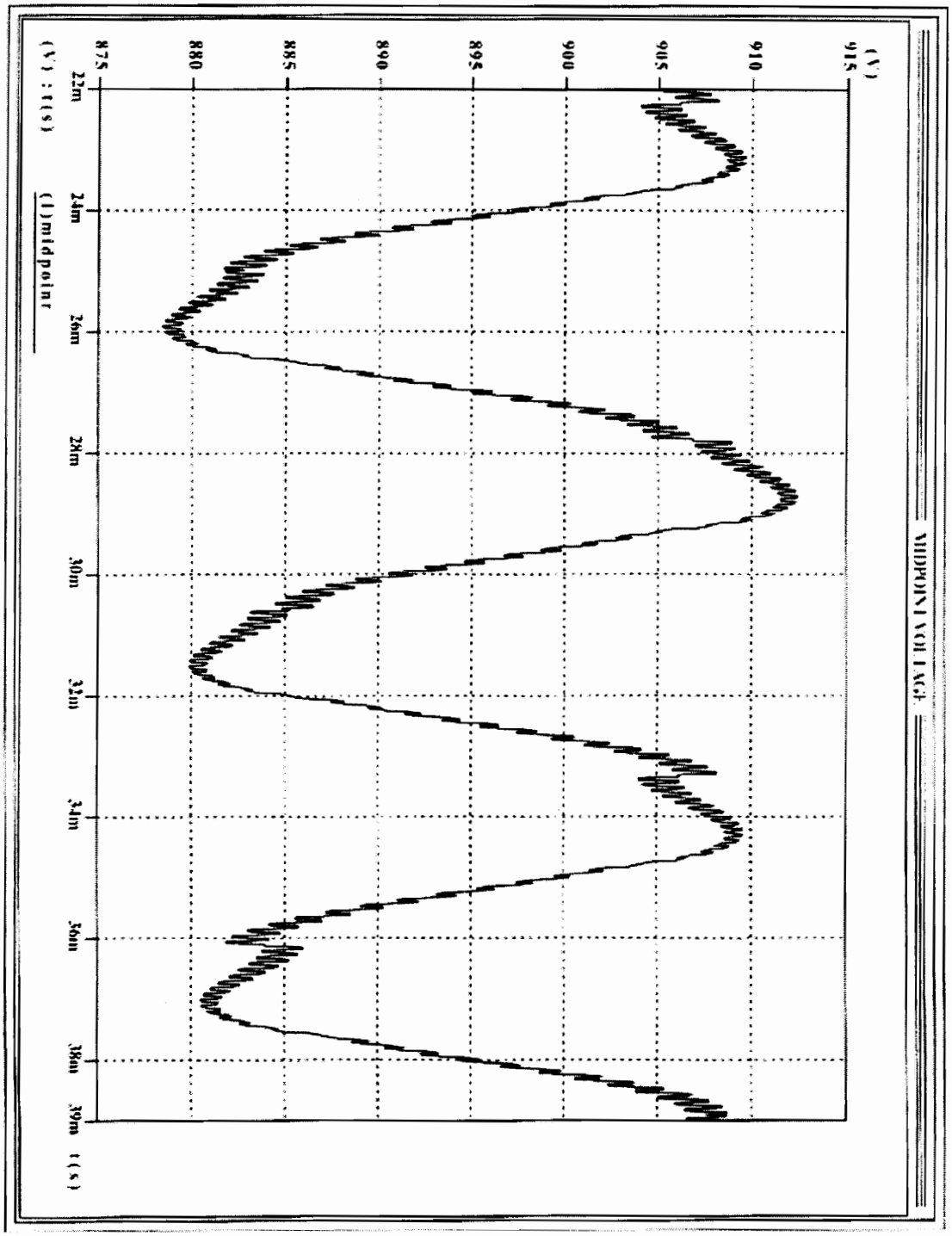

Fig. 3.9. Midpoint voltage, -v_n

This happens six times in one cycle since there are six medium vectors in one cycle, which results in a third order harmonic. Further improvements on SVM modulation can be done to reduce the magnitude of the low frequency harmonic.

An other important output of the simulation is the output current harmonics. Fig. 3.10. and 3.11. show the harmonics content of the output currents for low and high frequencies. It can be seen that the output current has a strong component at 60 Hz, and very weak 5^{th}, 7^{th}, 15^{th}, and 19^{th} harmonics. Other harmonics are at the multiples of switching frequency (10 kHz) and their size is determined by output filter design.

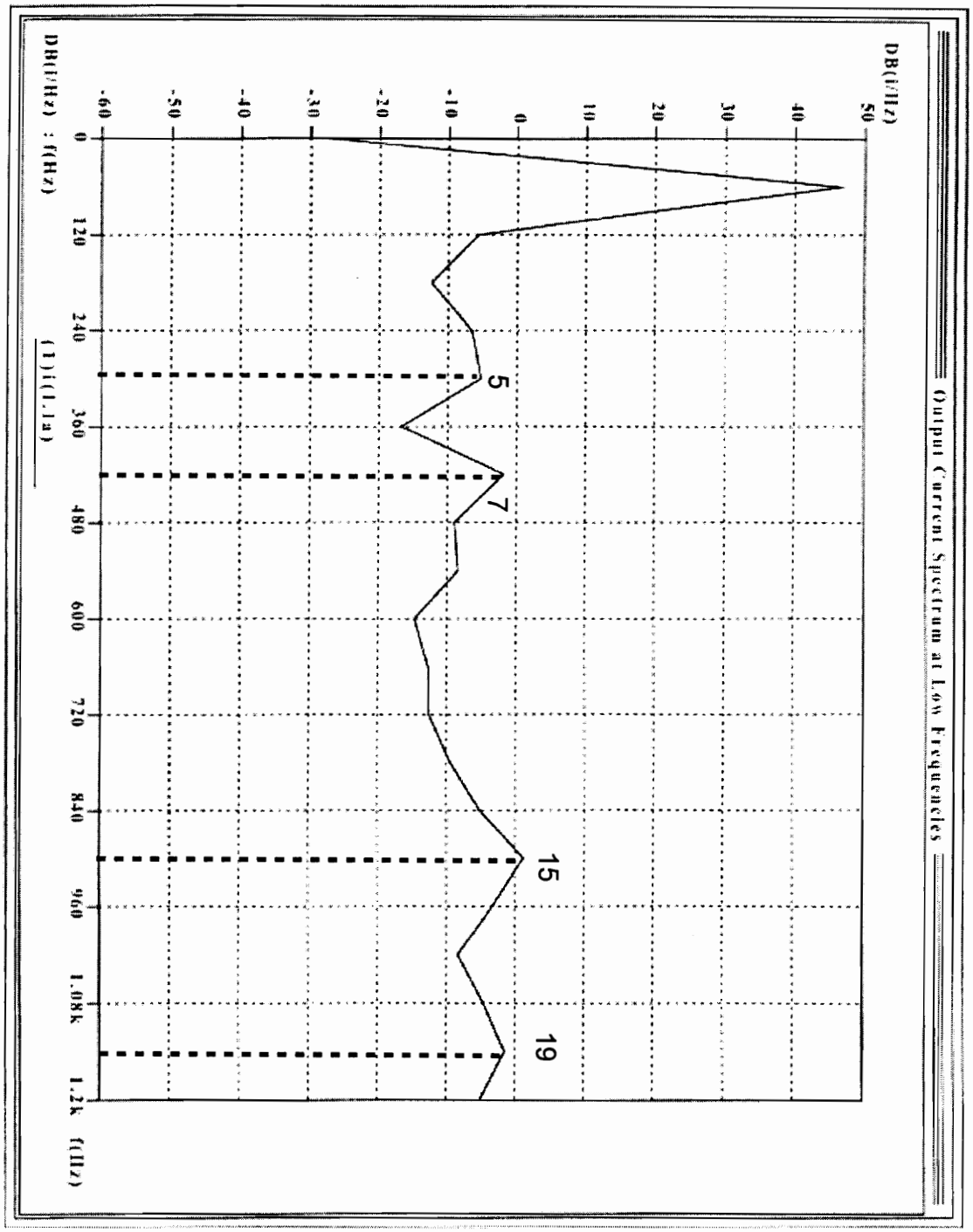

Fig. 3.10. Harmonic content of output current, i_a

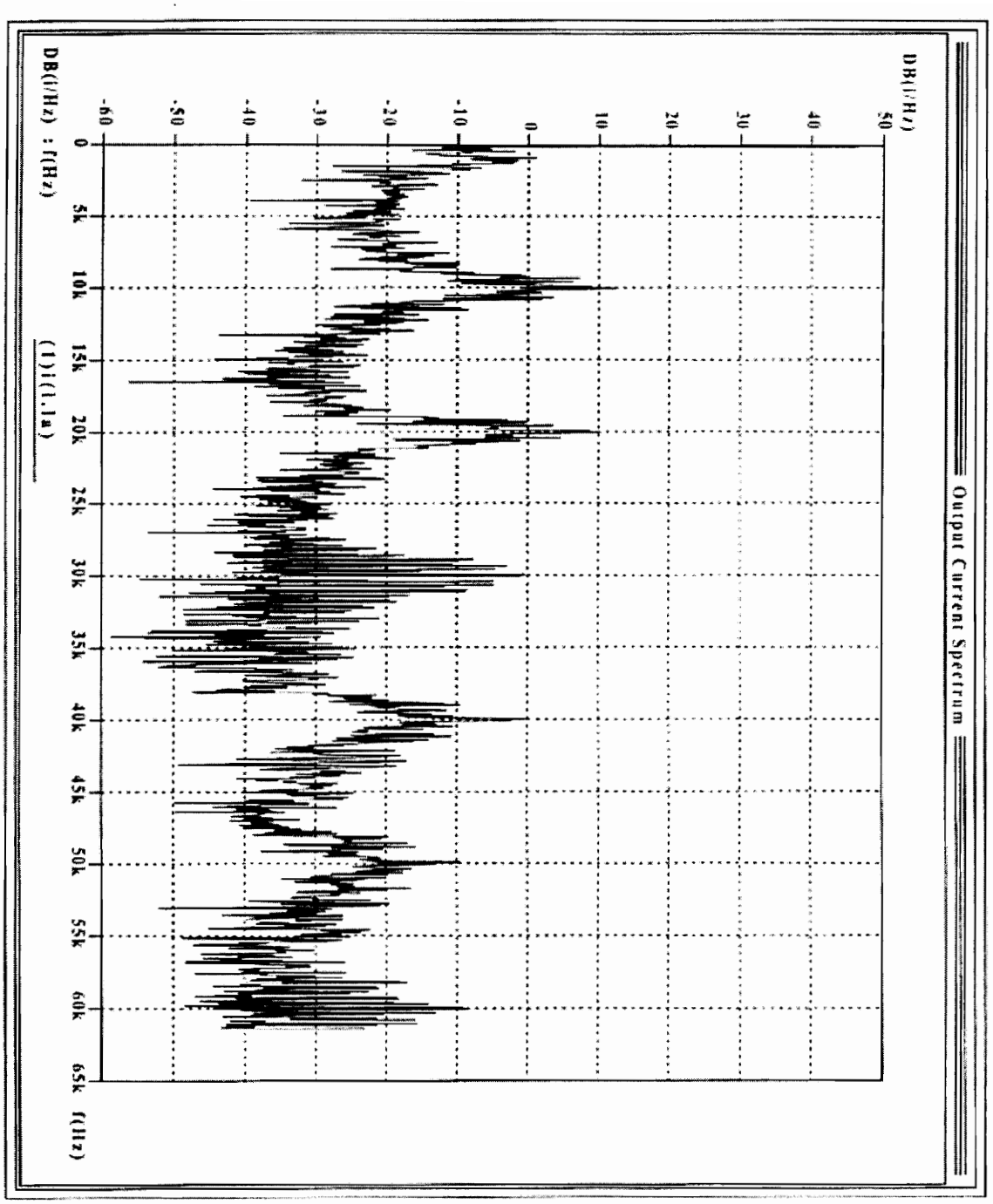

Fig. 3.11. Harmonic content of the output current, i_a

3.4 Conclusion

In this chapter, simulation of the three-phase, three-level VSI is given. First, SVM algorithm used to build the SABER files is proposed. Sector identification is explained for one sixty degree interval and the remaining sector identifications are given as flow charts in Appendix D. Second, all the input parameters for the simulation are given in detail. These parameters are especially important for the readers who wants to implement the program on a workstation or a DSP board. As a consequence, similar simulation can be done easily by changing the input parameters. Then, structure of the SABER simulation files is given for a better understanding of the simulation. Lastly, time domain simulation results are provided for a 250 kW voltage source inverter. Output line currents, line-to-line voltages, and midpoint voltages are obtained. In addition to that, output current harmonics are analyzed.

Simulation results shows that the proposed SVM algorithm for a three-phase three-level VSI works well. The same algorithm can be used in a Digital Signal Processing (DSP) board to develop a prototype circuit. Proposed algorithm and simulation reveals that the midpoint voltage is stable at a third order harmonic superimposed on top of the half of the dc-bus voltage. However, more analysis can be done to minimize the peak-to-peak ripple of third harmonic effect at midpoint which is 1. 66 % of the dc-bus voltage for above given operating conditions.

4. MODELING OF THREE-LEVEL VSIs

Average and small signal modeling of three-level VSIs is very important for control loop design of the converter and dynamic analysis of the system where three-level VSI is used.

A simple model of the three-level VSI and the load is given in [9-10]. This is a very simple description of the converter-load side behavior. However, the dynamic description of the dc-link side and load side are not covered in the literature. In this work, small-signal analysis of a three-phase three-level VSI which covers the dc-side and load-side dynamics is proposed [11].

Typical assumptions for a small-signal model are:

- perturbations are much smaller than the operating point values,
- switching frequency is much higher than the output line frequency (this is a requirement for average-model analysis), and
- all switches are assumed to be ideal and inductors, capacitors, etc. are considered to be time invariant.

There are certain steps to follow to obtain the small-signal model of a switching converter, Fig. 4.1.

First of all, switching function representation of the converter is proposed. Switching function is a discontinuous function of time which completely determines the input/output voltage/current relationships of the whole converter. In a simple dc/dc converter, switching function is a single function of time which takes the values of "1" and "0" meaning switch is "on" and "off", respectively. However, in a multiphase converter, since there are multiple input/output voltage and currents, the switching function must be a matrix.

Second, average model is obtained by applying the moving average operator to the switching function. This results in non-linear time varying systems equations. Then d-q-0 transformation eliminates the time variations and gives non-linear time invariant equations.

Finally, linearization of these equations around the operating point results in the linearized small-signal model. Desired transfer functions can be then easily obtained from small-signal equivalent circuit. Every block in Fig. 4.1. is explained in the following chapters.

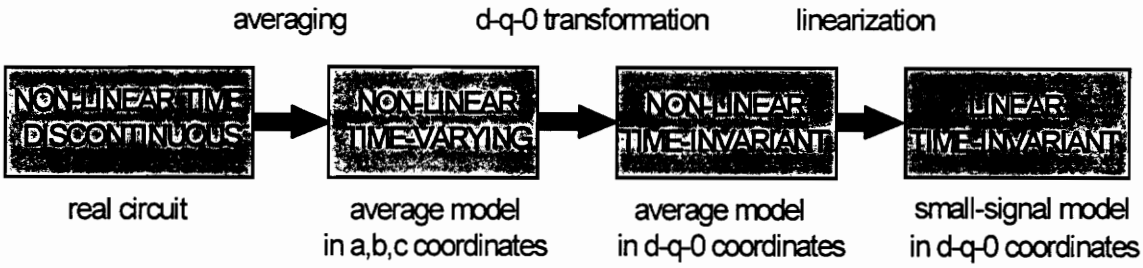

Fig. 4.1. Steps of obtaining the small-signal model of a three-phase converter.

4.1. Discontinuous Model Of The Converter

Input/output voltage and current relationship is derived in Chapter 2 as

$$\begin{bmatrix} vao \\ vbo \\ vco \end{bmatrix} = \begin{bmatrix} Sap & San \\ Sbp & Sbn \\ Scp & Scn \end{bmatrix} \cdot \begin{bmatrix} vp \\ vn \end{bmatrix} = [S] \cdot [vg] \quad \text{, and} \qquad (4.1)$$

$$\begin{bmatrix} ip \\ in \end{bmatrix} = [S]^T \cdot \begin{bmatrix} ia \\ ib \\ ic \end{bmatrix} \qquad (4.2)$$

which is the nonlinear time discontinuos model of the converter, i.e. the first block in Fig. 4.1. Note that since there are two input voltage sources, vp, vn, and three output voltages, the relationship between these two voltages must be a matrix with a dimension of 3X2. In addition to above equations, from Fig. 4.2., dynamic equations of input dc-capacitors can be written as:

$$idc = C_{dc} \frac{dvp}{dt} + ip = -C_{dc} \frac{dvn}{dt} - in, \qquad (4.3)$$

where $C_1 = C_2 = C_{dc}$. Assuming the L,C, and R are the same in every phase, the relationship between line-to-midpoint voltages and the voltage between output ground and midpoint, i.e. vNO , is

$$vNO = \frac{vao + vbo + vco}{3}. \qquad (4.4)$$

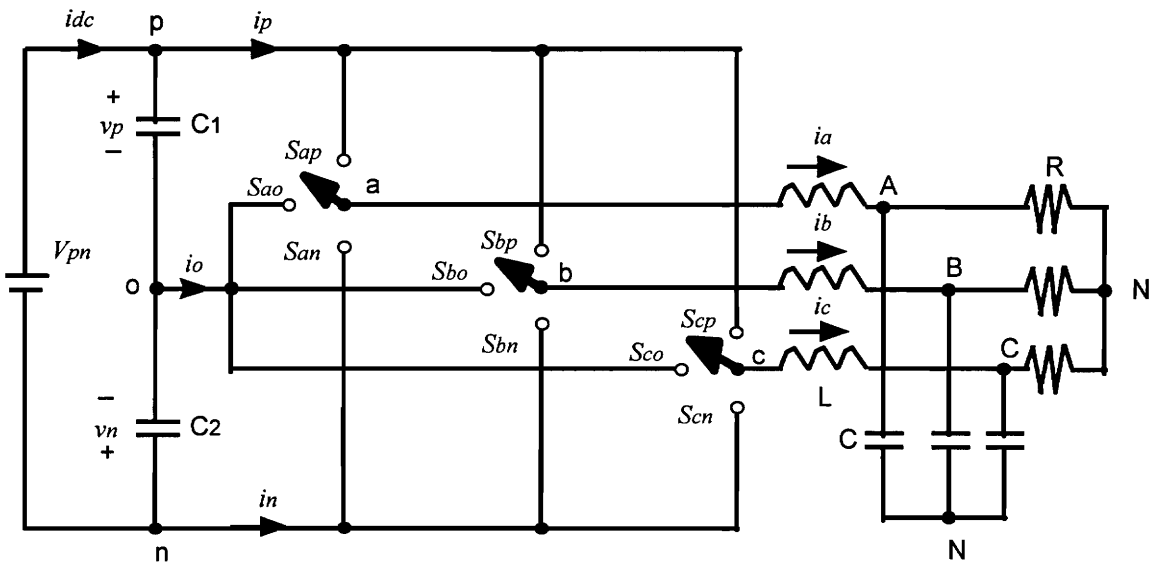

Fig. 4.2 Switching function representation of three-phase three-level VSI

4.2. Average Model

Moving average of a periodic function x(t) over one switching cycle is defined as:

$$\bar{x}(t) = \frac{1}{Tc} \cdot \int_{t-T_c}^{t} x(\tau) \cdot d\tau \tag{4.5}$$

where $x(t)$ represents the instantaneous value of currents or voltages [12]. Average model of three-level VSI is obtained by applying the moving average operator to (4.1) and (4.2), where input voltages vp , and vn are assumed to be constant over a switching period. Then, average model input-output voltage relationship is

$$\begin{bmatrix} \bar{v}ao \\ \bar{v}bo \\ \bar{v}co \end{bmatrix} = \begin{bmatrix} dap & dan \\ dbp & dbn \\ dcp & dcn \end{bmatrix} \cdot \begin{bmatrix} \bar{v}p \\ \bar{v}n \end{bmatrix} = [d] \cdot \begin{bmatrix} \bar{v}p \\ \bar{v}n \end{bmatrix} \tag{4.6}$$

where duty cycles dap, dbp, dcp are average three-phase duty cycles. Input-output current relationship becomes,

$$\begin{bmatrix} \bar{i}p \\ \bar{i}n \end{bmatrix} = [d]^T \cdot \begin{bmatrix} \bar{i}a \\ \bar{i}b \\ \bar{i}c \end{bmatrix} \quad , \tag{4.7}$$

where

$$\bar{i}p + \bar{i}n + \bar{i}o = 0 . \tag{4.8}$$

State equations with averaged current and voltage in a,b,c coordinates can be obtained by KVL and KCL from the circuit in Fig. 4.2. They can be written as:

$$\frac{d}{dt}\begin{bmatrix}\bar{x}i\\ \bar{x}v\end{bmatrix}=\begin{bmatrix}\mathbf{0}3x3 & -\frac{1}{L}I3x3\\ \frac{1}{C}I3x3 & -\frac{1}{R\cdot C}I3x3\end{bmatrix}\cdot\begin{bmatrix}\bar{x}i\\ \bar{x}v\end{bmatrix}+\begin{bmatrix}\frac{1}{L}I3x3\\ \mathbf{0}3x3\end{bmatrix}\cdot\begin{bmatrix}\bar{v}ao-\bar{v}NO\\ \bar{v}bo-\bar{v}NO\\ \bar{v}co-\bar{v}NO\end{bmatrix}, \text{ and}$$

$$\frac{d}{dt}\begin{bmatrix}\bar{v}p\\ \bar{v}n\end{bmatrix}=\begin{bmatrix}-\frac{1}{Cdc}dap & -\frac{1}{Cdc}dbp & -\frac{1}{Cdc}dcp\\ -\frac{1}{Cdc}dan & -\frac{1}{Cdc}dbn & -\frac{1}{Cdc}dcn\end{bmatrix}\cdot\bar{x}i+\begin{bmatrix}\frac{1}{Cdc}\\ -\frac{1}{Cdc}\end{bmatrix}\cdot\bar{i}dc, \tag{4.9}$$

where,

$$\bar{x}i=\begin{bmatrix}\bar{i}a\\ \bar{i}b\\ \bar{i}c\end{bmatrix}, \qquad \bar{x}v=\begin{bmatrix}\bar{v}AN\\ \bar{v}BN\\ \bar{v}CN\end{bmatrix} \tag{4.10}$$

are the average currents and voltages. In (4.9), 0_{3x3}, and I_{3x3} are 3x3 zero and identity matrices, respectively. From (4.9) average model circuit of a three-phase three-level VSI can be obtained as in Fig. 4.3. In average model, instead of output line-to-line voltages, line-to-midpoint voltages are considered to observe the midpoint dynamics.

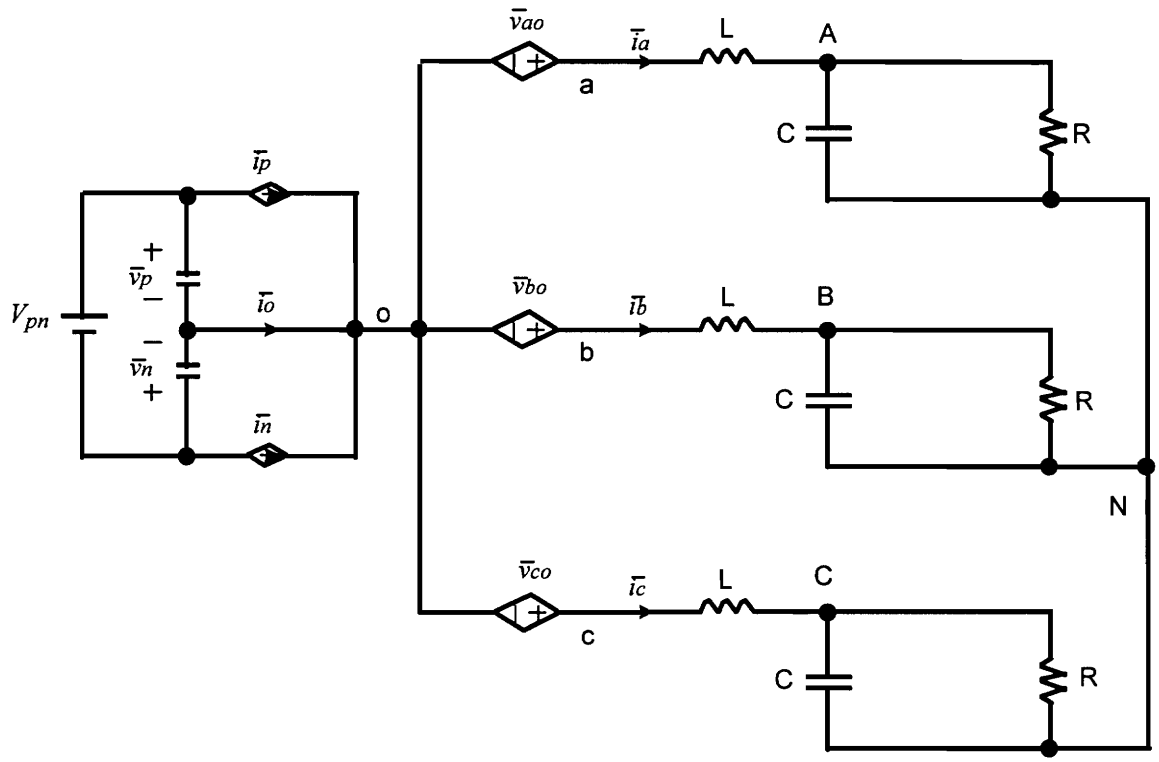

Fig. 4.3. Average circuit model of a three-phase three-level VSI

4.3 d-q-0 Transformation

4.3.1 State-Space Model in d-q-0 Coordinate Frame

D-q-0 model of the converter can be obtained by multiplying the both sides of (4.9) by transformation matrix T, which is defined as:

$$T(w_r t)=\sqrt{\frac{2}{3}}\begin{bmatrix} \cos(w_r t-\delta) & \cos(w_r t-2\pi/3-\delta) & \cos(w_r t-4\pi/3-\delta) \\ -\sin(w_r t-\delta) & -\sin(w_r t-2\pi/3-\delta) & -\sin(w_r t-4\pi/3-\delta) \\ 1/\sqrt{2} & 1/\sqrt{2} & 1/\sqrt{2} \end{bmatrix}, \quad (4.11)$$

where w_r is the angular frequency of the rotating d-q-0 frame, and δ is the phase shift between a,b,c and d-q-0 coordinates [10]. Note that matrix T is an orthonormal matrix, i.e. $T^T = T^{-1}$. When transformation is applied to (4.6) and (4.7), the relationships between input-output voltages and currents become

$$\begin{bmatrix} vd \\ vq \\ v0 \end{bmatrix} = \begin{bmatrix} dpd & dnd \\ dpq & dnq \\ dp0 & dn0 \end{bmatrix} \cdot \begin{bmatrix} \bar{v}p \\ \bar{v}n \end{bmatrix}, \text{ and} \quad (4.12)$$

$$\begin{bmatrix} \bar{i}p \\ \bar{i}n \end{bmatrix} = \begin{bmatrix} dpd & dpq & dp0 \\ dnd & dnq & dn0 \end{bmatrix} \cdot \begin{bmatrix} iYd \\ iYq \\ iY0 \end{bmatrix}, \quad (4.13)$$

where

$$\begin{bmatrix} vd \\ vq \\ v0 \end{bmatrix}, \quad \begin{bmatrix} iYd \\ iYq \\ iY0 \end{bmatrix}, \text{and} \quad \begin{bmatrix} dpd & dnd \\ dpq & dnq \\ dp0 & dn0 \end{bmatrix}$$

are the d-q-0 transformation of

$$\begin{bmatrix} \bar{v}ao \\ \bar{v}bo \\ \bar{v}co \end{bmatrix}, \quad \begin{bmatrix} \bar{i}a \\ \bar{i}b \\ \bar{i}c \end{bmatrix}, \text{and} \quad \begin{bmatrix} dap & dan \\ dbp & dbn \\ dcp & dcn \end{bmatrix}$$

respectively. The following assumptions are considered while average model of three-level converter is obtained in d-q-0 coordinates.

- Load and low-pass filter components are symmetric, i.e. $iY0 = 0$ and $vY0 = 0$, and
- "p" and "n" rail duty cycles are assumed to be equal and with a 180° phase shift.

State-space model of three-level VSI in d-q-0 coordinate frame can be written as:

$$\frac{d}{dt}\begin{bmatrix} iYd \\ vYd \\ iYq \\ vYq \\ vp \\ vn \end{bmatrix} = \begin{bmatrix} 0 & -1/L & \omega_r & 0 & dpd/L & dnd/L \\ 1/C & -1/RC & 0 & \omega_r & 0 & 0 \\ -\omega_r & 0 & 0 & -1/L & dpq/L & dnq/L \\ 0 & -\omega_r & 1/C & -1/RC & 0 & 0 \\ -dpd/Cdc & 0 & -dpq/Cdc & 0 & 0 & 0 \\ -dnd/Cdc & 0 & -dnq/Cdc & 0 & 0 & 0 \end{bmatrix} \cdot \begin{bmatrix} iYd \\ vYd \\ iYq \\ vYq \\ vp \\ vn \end{bmatrix} + \begin{bmatrix} 0 \\ 0 \\ 0 \\ 0 \\ 1/Cdc \\ -1/Cdc \end{bmatrix} \cdot idc \tag{4.14}$$

where d-q-0 components of output voltage and currents, and input capacitor voltages are chosen as state variables. Selection of the output variables depend on what to control. Output voltage d and q components and one input capacitor voltage are chosen as the output variables. Output function can be written as:

$$\begin{bmatrix} vYd \\ vYq \\ \overline{v}p \end{bmatrix} = \begin{bmatrix} 0 & 1 & 0 & 0 & 0 & 0 \\ 0 & 0 & 0 & 1 & 0 & 0 \\ 0 & 0 & 0 & 0 & 1 & 0 \end{bmatrix} \cdot \begin{bmatrix} iYd \\ vYd \\ iYq \\ vYq \\ \overline{v}_p \\ \overline{v}_n \end{bmatrix} \tag{4.15.}$$

where

$$\begin{bmatrix} vYd \\ vYq \\ vY0 \end{bmatrix}$$

is the d-q-0 transformation of

$$\begin{bmatrix} \overline{v}AN \\ \overline{v}BN \\ \overline{v}CN \end{bmatrix}$$

and $vY0 = 0$ since the three phase output voltages are assumed to be balanced.

4.3.2 Steady State Solutions

Steady state solutions for equations (4.14) and (4.15) can be obtained by setting the dynamic terms to zero. The results are given in (4.16), (4.17), (4.18), and Table 4. Note that, capital letters are used to denote the steady state solutions.

$$Dd = Dpd = -Dnd, \tag{4.16}$$

$$Dq = Dpq = -Dnq, \tag{4.17}$$

$$D0 = Dp0 = Dn0, \tag{4.18}$$

Table 4 Steady state solutions

d component of the duty cycle	$Dd = \frac{VYd \cdot \left(1 - \omega_r{}^2 LC\right) - VYq \cdot \frac{\omega_r L}{R}}{Vpn}$
q component of the duty cycle	$Dq = \frac{VYd \cdot \frac{\omega_r L}{R} + VYq \cdot \left(1 - \omega_r{}^2 LC\right)}{Vpn}$
zero component of the duty cycle	$D0 = \sqrt{2\left(Dd^2 + Dq^2\right)}$
d component of the output current	$IYd = \frac{VYd}{R} + \omega_r C \cdot VYq$
q component of the output current	$IYq = \frac{VYq}{R} + \omega_r C \cdot VYd$
zero component of the output current	$IY0 = 0$

Input side currents and output voltages in steady state are derived the same way, Table 5.

Table 5 Steady state solutions for input side

p rail current	$Ip = Dd \cdot Id + Dq \cdot Iq$
n rail current	$In = -Ip$
midpoint current	$Io = 0$
d component of the output voltage	$VYd = Dd \cdot Vpn$
q component of the output voltage	$VYq = Dq \cdot Vpn$
zero component of the output voltage	$VY0 = 0$
voltage between N and midpoint	$VNo = 0$
upper capacitor voltage	$Vp = -Vn = \frac{Vpn}{2}$
voltage ripple in midpoint	$Vp + Vn = 0$

Average circuit model of three-level VSI in d-q-0 coordinates is given in Fig. 4.4.

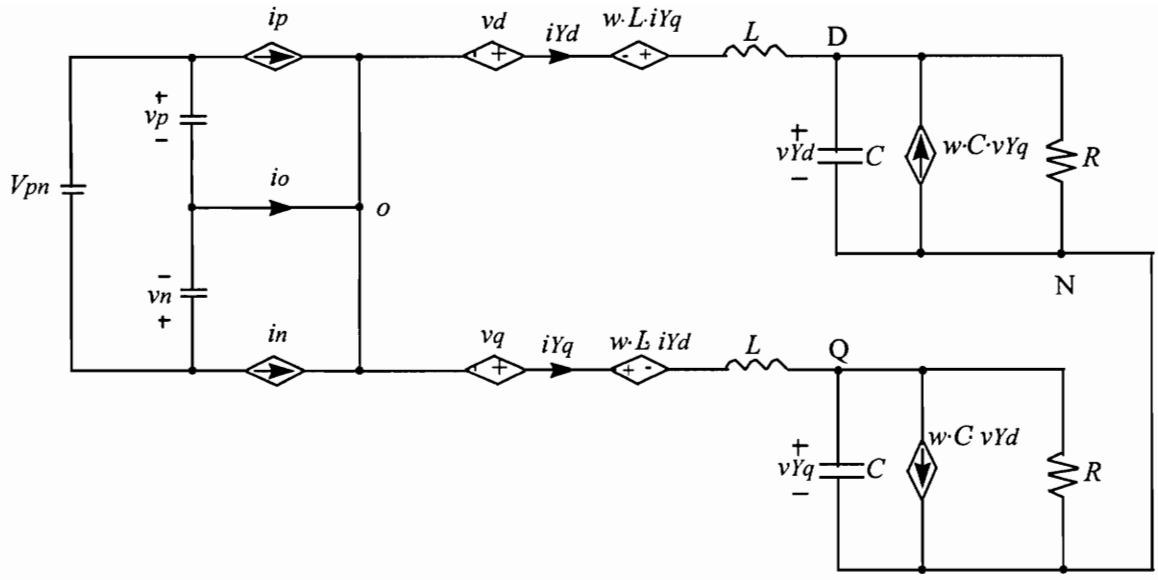

Fig. 4.4. Average circuit model in d-q-0 coordinates

4.4 Small-Signal Model

Small signal model of three-level VSI can be obtained from (4.14) and (4.15) by perturbing the voltage and current around the operating point [10]. Capital letters denote the operating point value and $(\hat{\cdot})$ represents the small-signal quantities. Small-signal equations can be written as:

$$s\begin{bmatrix}\hat{i}_{Yd}\\ \hat{v}_{Yd}\\ \hat{i}_{Yq}\\ \hat{v}_{Yq}\\ \hat{v}_{p}\\ \hat{v}_{n}\end{bmatrix}=\begin{bmatrix}0 & -1/L & \omega_r & 0 & Dpd/L & Dnd/L\\ 1/C & -1/RC & 0 & \omega_r & 0 & 0\\ -\omega_r & 0 & 0 & -1/L & Dpq/L & Dnq/L\\ 0 & -\omega_r & 1/C & -1/RC & 0 & 0\\ -Dpd/C_{dc} & 0 & -Dpq/C_{dc} & 0 & 0 & 0\\ -Dnd/C_{dc} & 0 & -Dnq/C_{dc} & 0 & 0 & 0\end{bmatrix}\cdot\begin{bmatrix}\hat{i}_{Yd}\\ \hat{v}_{Yd}\\ \hat{i}_{Yq}\\ \hat{v}_{Yq}\\ \hat{v}_{p}\\ \hat{v}_{n}\end{bmatrix}+$$

$$\begin{bmatrix}V_p/L & V_n/L & 0 & 0\\ 0 & 0 & 0 & 0\\ 0 & 0 & V_p/L & V_n/L\\ 0 & 0 & 0 & 0\\ -I_{Yd}/C_{dc} & 0 & -I_{Yq}/C_{dc} & 0\\ 0 & -I_{Yd}/C_{dc} & 0 & -I_{Yq}/C_{dc}\end{bmatrix}\cdot\begin{bmatrix}\hat{d}_{pd}\\ \hat{d}_{nd}\\ \hat{d}_{pq}\\ \hat{d}_{nq}\end{bmatrix}+\begin{bmatrix}0\\ 0\\ 0\\ 0\\ 1/C_{dc}\\ -1/C_{dc}\end{bmatrix}\cdot\hat{i}_{dc} \quad \text{and (4.19)}$$

$$\begin{bmatrix}\hat{v}_{Yd}\\ \hat{v}_{Yq}\\ \hat{v}_{p}\end{bmatrix}=\begin{bmatrix}0 & 1 & 0 & 0 & 0 & 0\\ 0 & 0 & 0 & 1 & 0 & 0\\ 0 & 0 & 0 & 0 & 1 & 0\end{bmatrix}\cdot\begin{bmatrix}\hat{i}_{Yd}\\ \hat{v}_{Yd}\\ \hat{i}_{Yq}\\ \hat{v}_{Yq}\\ \hat{v}_{p}\\ \hat{v}_{n}\end{bmatrix}. \qquad (4.20)$$

Any desired transfer function for controller design can be obtained from (4.19) and (4.20) easily.

4.5 Bode Plots of Transfer Functions

Small-signal model of the three-level converter is a sixth order system. That is why it is very difficult to obtain the analytical expressions for transfer functions. Instead of that, state-space matrices are used to get the desired bode plots. MatLab program is used to obtain the Bode plots. The parameters in Table 6 are chosen as the operating point values.

Note that, parameters in Table 6 are the same parameters as in SABER simulation. Two transfer functions are given in Fig. 4.5. These transfer functions give the information about the poles, zeros, and the dc-gain which are necessary for the control loop design. The rest of the transfer functions are given in Appendix E.

In order to verify the circuit model in Fig. 4.4, a PSPICE [13] simulation is performed by using the parameters given in Table 6. The linearization was done by PSPICE program. The simulation results and files are presented in Appendix F. The frequency response given in Fig. 4.5(b) matches with the simulation results given in Appendix F.

Table 6 Operating point values for small-signal analysis

dc-link voltage	V_{pn}=1800 V
power level	Po=250 kW
line current current	I_a=210 A
balanced resistive load	$R = 4.6\ \Omega$
output inductor	L=0.25 mH
output capacitor	C=100 uF
dc-link capacitors	C_1=C_2=C_{dc}=1 mF

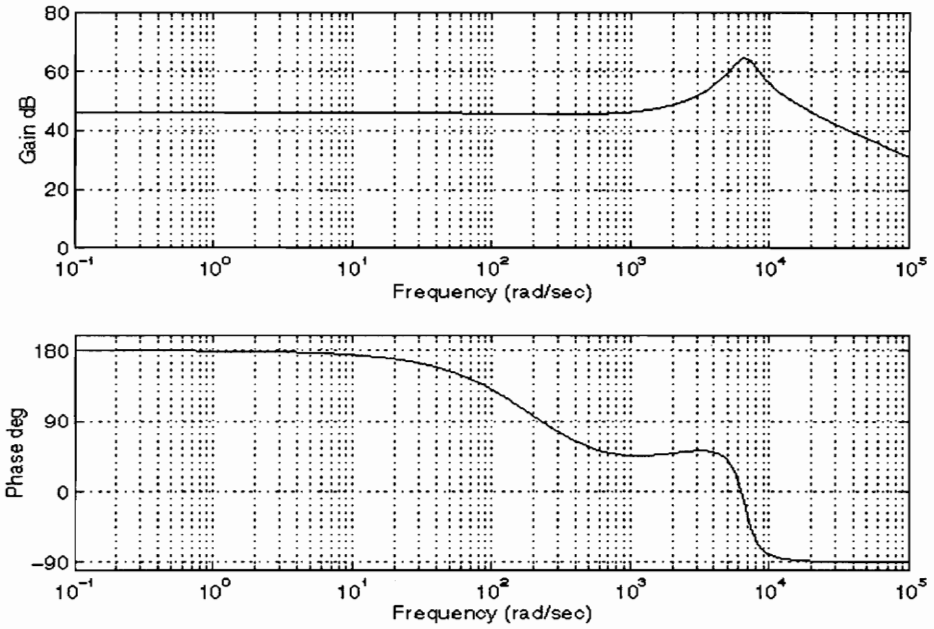

Fig. 4.5. (a) Frequency response of $\hat{i}_{Yd}/\hat{d}_{pd}$.

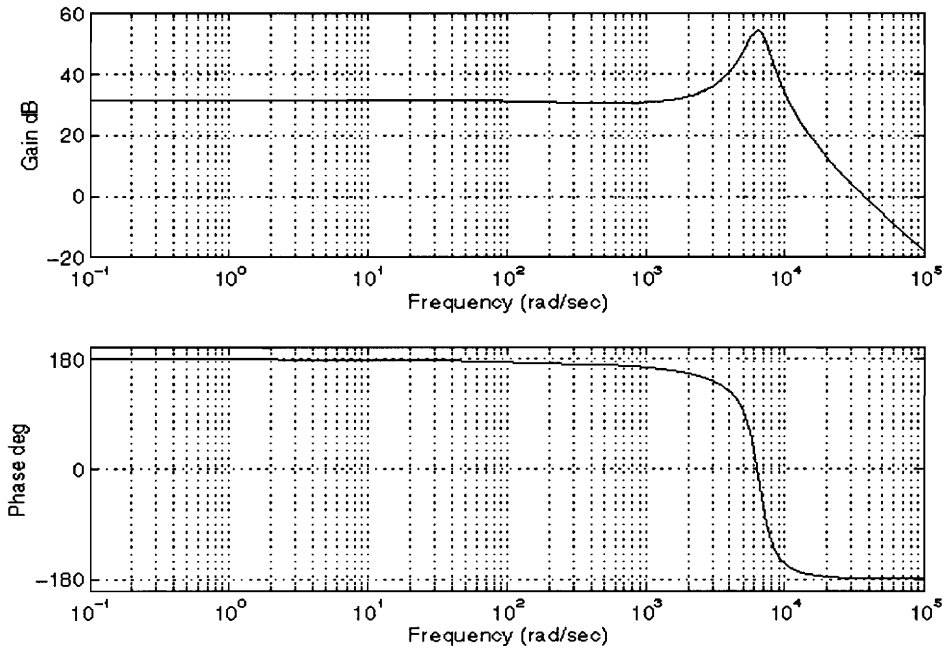

Fig. 4.5.(b) Frequency response of $\hat{i}_{Yd}/\hat{d}_{pq}$.

4.6 Conclusions

In this chapter, average and small-signal analysis of the three-phase three-level VSI were developed for the first time. Switching function representation, and average models in a,b,c and d-q-0 coordinates are derived. Several transfer functions are obtained from small-signal equivalent circuit. Control variables of the model are the duty cycles of single-pole-triple-throw switches. Two duty cycles from each single-pole-triple-throw switch should be known, which results in total six control variables. As of the output variable, two output line-to-line voltages, or currents, and two input capacitors voltages can be controlled.

Contribution to this point is the development of SVM algorithm, verification of the algorithm by SABER simulation and development of the small-signal modeling of the converter. However, for a complete closed-loop analysis, and system level experiments, an error compensator and small-signal model of SVM block need to be investigated as future work.

5. SUMMARY AND FUTURE WORK

Three-phase three-level voltage source inverters (VSIs) are very attractive for high-voltage and high-power applications. The most important advantages of a three-level VSI compared with a conventional two-level VSI, for the same power level and switching frequency are:

- only half of the dc-link voltage is applied to the switches,
- switching losses are reduced, and
- output harmonics are reduced.

The disadvantages of a three-level VSI are high number of devices and voltage balance of the dc-link capacitors.

In this work, three-phase three-level VSI are investigated. Operation principle of the converter is explained by switching functions. There are three output voltages and two input voltages. The functional relationship between input and output voltages must be a matrix of 3x2. Note that in a conventional two-level VSI this relationship is a 3x1 array.

Space Vector Modulation (SVM) of three-level VSI is proposed. There are total 3 zero and 24 non-zero switching vectors. Which vector to chose is a very important subject. To achieve sector identification, a modulation algorithm is proposed. Duty cycle calculations for all sectors is given. A Digital Signal Processor can be used in order to calculate the duty cycles in the application.

A comprehensive SABER program is developed to verify the proposed SVM algorithm. Algorthm is tested in a 250 kW three-phase three-level VSI. All duty cycle calculations and flow chart of the algorithm is given in Appendixes B and D. Simulation results reveal that the proposed modulation scheme and

algorithm works well. There is a low frequency voltage fluctuation in the midpoint with a peak-to-peak voltage less than 2 % of dc-link voltage. Third order voltage swing is caused by the usage of medium vectors. However, small signal modeling reveals that this peak-to-peak voltage swing can be further reduced.

The future work is to optimize the SVM algorithm to further minimize the midpoint voltage. For the closed-loop operation, a feedback error amplifier can be designed based on the small signal model and the small-signal model of SVM block can be derived.

APPENDIX A: SEQUENCE OF THE VECTORS FOR EACH SECTOR

	j=1	j=2	j=3	j=4
	V_{O1p} poo	**V_{O1p}** poo	**V_{O2p}** ppo	**V_{01p}** poo
i=2	**V_{12}** pon	**V_{12}** pon	**V_{2}** ppn	**V_{0}** ooo
	V_{1} pnn	**V_{02n}** oon	**V_{12}** pon	**V_{02n}** oon
	V_{O1n} onn	**V_{O1n}** onn	**V_{O2n}** oon	**V_{O1n}** onn

	j=1	j=2	j=3	j=4
	V_{O2n} oon	**V_{O2n}** oon	**V_{O3n}** non	**V_{02n}** oon
i=3	**V_{23}** opn	**V_{23}** opn	**V_{3}** npn	**V_{0}** ooo
	V_{2} ppn	**V_{03p}** opo	**V_{23}** opn	**V_{03p}** opo
	V_{O2p} ppo	**V_{O2p}** ppo	**V_{O3p}** opo	**V_{O2p}** ppo

	j=1	j=2	j=3	j=4
	V_{O3p} opo	**V_{O3p}** opo	**V_{O4p}** opp	**V_{03p}** opo
i=4	**V_{34}** npo	**V_{34}** npo	**V_{4}** npp	**V_{0}** ooo
	V_{3} npn	**V_{04n}** noo	**V_{34}** npo	**V_{04n}** noo
	V_{O3n} non	**V_{O3n}** non	**V_{O4n}** noo	**V_{O3n}** non

	j=1	j=2	j=3	j=4
	VO4n noo	**VO4n** noo	**VO5n** nno	**V04n** noo
i=5	**V45** nop	**V45** nop	**V5** nnp	**V0** ooo
	V4 npp	**V05p** oop	**V45** nop	**V05p** oop
	VO4p opp	**VO4p** opp	**VO5p** oop	**VO4p** opp

	j=1	j=2	j=3	j=4
	VO5p oop	**VO5p** oop	**VO6p** pop	**V05p** oop
i=6	**V56** onp	**V56** onp	**V6** pnp	**V0** ooo
	V5 nnp	**V06n** ono	**V56** onp	**V06n** ono
	VO5n nno	**VO5n** nno	**VO6n** ono	**VO5n** nno

	j=1	j=2	j=3	j=4
	VO6n ono	**VO6n** ono	**VO1n** onn	**V06n** ono
i=1	**V61** pno	**V61** pno	**V1** pnn	**V0** ooo
	V6 pop	**V01p** poo	**V61** pno	**V01p** poo
	VO6p opp	**VO6p** pop	**VO1p** poo	**VO6p** pop

APPENDIX B: DUTY CYCLE CALCULATIONS

$$\left(dm = \frac{\sqrt{3}}{2} \cdot D \bmod \right)$$

i=2, j=1
$t_{01} = 2 \cdot T_s \cdot (1 - dm \cdot \cos(\theta - 30^o) - \frac{dm \cdot \sin(\theta - 30^o)}{\sqrt{3}})$
$t_1 = T_s \cdot (-1 + 2 \cdot dm \cdot \cos(\theta - 30^o) - \frac{2 \cdot dm \cdot \sin(\theta - 30^o)}{\sqrt{3}})$
$t_{12} = T_s \cdot (\frac{4 \cdot dm \cdot \sin(\theta - 30^o)}{\sqrt{3}})$

i=2, j=2
$t_{01} = T_s \cdot (1 - \frac{4 \cdot dm \cdot \sin(\theta - 30^o)}{\sqrt{3}})$
$t_{12} = T_s \cdot (-1 + 2 \cdot dm \cdot \cos(\theta - 30^o) + \frac{2 \cdot dm \cdot \sin(\theta - 30^o)}{\sqrt{3}})$
$t_{02} = T_s \cdot (1 - 2 \cdot dm \cdot \cos(\theta - 30^o) + \frac{2 \cdot dm \cdot \sin(\theta - 30^o)}{\sqrt{3}})$

i=2, j=3
$t_{02} = 2 \cdot T_s \cdot (1 - dm \cdot \cos(\theta - 30^o) - \frac{dm \cdot \sin(\theta - 30^o)}{\sqrt{3}})$
$t_2 = T_s \cdot (-1 + \frac{4 \cdot dm \cdot \sin(\theta - 30^o)}{\sqrt{3}})$
$t_{12} = T_s \cdot (2 \cdot dm \cdot \cos(\theta - 30^o) - \frac{2 \cdot dm \cdot \sin(\theta - 30^o)}{\sqrt{3}})$

i=2, j=4
$t_{01} = T_s \cdot (2 \cdot dm \cdot \cos(\theta - 30^o) - \frac{2 \cdot dm \cdot \sin(\theta - 30^o)}{\sqrt{3}})$
$t_{02} = T_s \cdot (\frac{4 \cdot dm \cdot \sin(\theta - 30^o)}{\sqrt{3}})$
$t_0 = T_s - t_{01} - t_{02}$

i=3, j=1
$t_{02} = 2 \cdot T \cdot_s (1 - \frac{2 \cdot dm \cdot \sin(\theta - 30^o)}{\sqrt{3}})$
$t_2 = T_s \cdot (-1 + 2 \cdot dm \cdot \cos(\theta - 30^o) + \frac{2 \cdot dm \cdot \sin(\theta - 30^o)}{\sqrt{3}})$
$t_{23} = T_s \cdot (\frac{2 \cdot dm \cdot \sin(\theta - 30^o)}{\sqrt{3}} - 2 \cdot dm \cdot \cos(\theta - 30^o))$

i=3, j=2
$t_{02} = T_s \cdot (1 - \frac{2 \cdot dm \cdot \sin(\theta - 30^o)}{\sqrt{3}} + 2 \cdot dm \cdot \cos(\theta - 30^o))$
$t_{03} = T_s \cdot (1 - 2 \cdot dm \cdot \cos(\theta - 30^o) - \frac{2 \cdot dm \cdot \sin(\theta - 30^o)}{\sqrt{3}})$
$t_{23} = T_s \cdot (-1 + \frac{4 \cdot dm \cdot \sin(\theta - 30^o)}{\sqrt{3}})$

i=3, j=3
$t_{03} = 2 \cdot T_s \cdot (1 - \frac{2 \cdot dm \cdot \sin(\theta - 30^o)}{\sqrt{3}})$
$t_{23} = T_s \cdot (\frac{2 \cdot dm \cdot \sin(\theta - 30^o)}{\sqrt{3}} + 2 \cdot dm \cdot \cos(\theta - 30^o))$
$t_3 = T_s \cdot (-2 \cdot dm \cdot \cos(\theta - 30^o) + \frac{2 \cdot dm \cdot \sin(\theta - 30^o)}{\sqrt{3}} - 1)$

i=3, j=4
$t_{01} = T_s \cdot (2 \cdot dm \cdot \cos(\theta - 30^o) + \frac{2 \cdot dm \cdot \sin(\theta - 30^o)}{\sqrt{3}})$
$t_{02} = T_s \cdot (\frac{2 \cdot dm \cdot \sin(\theta - 30^o)}{\sqrt{3}} - 2 \cdot dm \cdot \cos(\theta - 30^o))$
$t_0 = T_s - t_{01} - t_{02}$

i=4, j=1
$t_{03} = T_s \cdot (2 + 2 \cdot dm \cdot \cos(\theta - 30^o) - \frac{2 \cdot dm \cdot \sin(\theta - 30^o)}{\sqrt{3}})$
$t_3 = T_s \cdot (\frac{4 \cdot dm \cdot \sin(\theta - 30^o)}{\sqrt{3}} - 1)$
$t_{34} = T_s \cdot (-2 \cdot dm \cdot \cos(\theta - 30^o) - \frac{2 \cdot dm \cdot \sin(\theta - 30^o)}{\sqrt{3}})$

i=4, j=2
$t_{03} = T_s \cdot (2 \cdot dm \cdot \cos(\theta - 30^o) + \frac{2 \cdot dm \cdot \sin(\theta - 30^o)}{\sqrt{3}} + 1)$
$t_{04} = T_s \cdot (1 - \frac{4 \cdot dm \cdot \sin(\theta - 30^o)}{\sqrt{3}})$
$t_{34} = T_s \cdot (-1 + \frac{2 \cdot dm \cdot \sin(\theta - 30^o)}{\sqrt{3}} - 2 \cdot dm \cdot \cos(\theta - 30^o))$

i=4, j=3
$t_{04} = T_s \cdot (2 + 2 \cdot dm \cdot \cos(\theta - 30^o) - \frac{2 \cdot dm \cdot \sin(\theta - 30^o)}{\sqrt{3}})$
$t_{34} = T_s \cdot (\frac{4 \cdot dm \cdot \sin(\theta - 30^o)}{\sqrt{3}})$
$t_4 = T_s \cdot (-2 \cdot dm \cdot \cos(\theta - 30^o) - \frac{2 \cdot dm \cdot \sin(\theta - 30^o)}{\sqrt{3}} - 1)$

i=4, j=4
$t_{01} = T_s \cdot (\frac{4 \cdot dm \cdot \sin(\theta - 30^o)}{\sqrt{3}})$
$t_{02} = T_s \cdot (-2 \cdot dm \cdot \cos(\theta - 30^o) - \frac{2 \cdot dm \cdot \sin(\theta - 30^o)}{\sqrt{3}})$
$t_0 = 1 - t_{01} - t_{02}$

i=5, j=1
$t_{04} = T_s \cdot (2 + 2 \cdot dm \cdot \cos(\theta - 30^o) + \frac{2 \cdot dm \cdot \sin(\theta - 30^o)}{\sqrt{3}})$
$t_4 = T_s \cdot (\frac{2 \cdot dm \cdot \sin(\theta - 30^o)}{\sqrt{3}} - 2 \cdot dm \cdot \cos(\theta - 30^o) - 1)$
$t_{45} = T_s \cdot (-\frac{4 \cdot dm \cdot \sin(\theta - 30^o)}{\sqrt{3}})$

i=5, j=2
$t_{04} = T_s \cdot (1 + \frac{4 \cdot dm \cdot \sin(\theta - 30^o)}{\sqrt{3}})$
$t_{05} = T_s \cdot (1 + 2 \cdot dm \cdot \cos(\theta - 30^o) - \frac{2 \cdot dm \cdot \sin(\theta - 30^o)}{\sqrt{3}})$
$t_{45} = T_s \cdot (-1 - 2 \cdot dm \cdot \cos(\theta - 30^o) - \frac{2 \cdot dm \cdot \sin(\theta - 30^o)}{\sqrt{3}})$

i=5, j=3
$t_{05} = T_s \cdot (2 + 2 \cdot dm \cdot \cos(\theta - 30^o) + \frac{2 \cdot dm \cdot \sin(\theta - 30^o)}{\sqrt{3}})$
$t_{45} = T_s \cdot (\frac{2 \cdot dm \cdot \sin(\theta - 30^o)}{\sqrt{3}} - 2 \cdot dm \cdot \cos(\theta - 30^o))$
$t_5 = T_s \cdot (-1 - \frac{4 \cdot dm \cdot \sin(\theta - 30^o)}{\sqrt{3}})$

i=5, j=4
$t_{01} = T_s \cdot (-2 \cdot dm \cdot \cos(\theta - 30^o) + \frac{2 \cdot dm \cdot \sin(\theta - 30^o)}{\sqrt{3}})$
$t_{02} = T_s \cdot (-\frac{4 \cdot dm \cdot \sin(\theta - 30^o)}{\sqrt{3}})$
$t_0 = T_s - t_{01} - t_{02}$

i=6, j=1
$t_{05} = T_s \cdot (2 + \frac{4 \cdot dm \cdot \sin(\theta - 30^o)}{\sqrt{3}})$
$t_5 = T_s \cdot (-1 - \frac{2 \cdot dm \cdot \sin(\theta - 30^o)}{\sqrt{3}} - 2 \cdot dm \cdot \cos(\theta - 30^o))$
$t_{56} = T_s \cdot (2 \cdot dm \cdot \cos(\theta - 30^o) - \frac{2 \cdot dm \cdot \sin(\theta - 30^o)}{\sqrt{3}})$

i=6, j=2
$t_{05} = T_s \cdot (1 - 2 \cdot dm \cdot \cos(\theta - 30^o) + \frac{2 \cdot dm \cdot \sin(\theta - 30^o)}{\sqrt{3}})$
$t_{06} = T_s \cdot (1 + 2 \cdot dm \cdot \cos(\theta - 30^o) + \frac{2 \cdot dm \cdot \sin(\theta - 30^o)}{\sqrt{3}})$
$t_{56} = T_s \cdot (-1 - \frac{4 \cdot dm \cdot \sin(\theta - 30^o)}{\sqrt{3}})$

i=6, j=3
$t_{06} = T_s \cdot (2 + \frac{4 \cdot dm \cdot \sin(\theta - 30^o)}{\sqrt{3}})$
$t_{56} = T_s \cdot (-2 \cdot dm \cdot \cos(\theta - 30^o) - \frac{2 \cdot dm \cdot \sin(\theta - 30^o)}{\sqrt{3}})$
$t_6 = T_s \cdot (-1 + 2 \cdot dm \cdot \cos(\theta - 30^o) - \frac{2 \cdot dm \cdot \sin(\theta - 30^o)}{\sqrt{3}})$

i=6, j=4
$t_{01} = T_s \cdot (-2 \cdot dm \cdot \cos(\theta - 30^o) - \frac{2 \cdot dm \cdot \sin(\theta - 30^o)}{\sqrt{3}})$
$t_{02} = T_s \cdot (2 \cdot dm \cdot \cos(\theta - 30^o) - \frac{2 \cdot dm \cdot \sin(\theta - 30^o)}{\sqrt{3}})$
$t_0 = T_s - t_{01} - t_{02}$

i=1, j=1
$t_{06} = T_s \cdot (2 - 2 \cdot dm \cdot \cos(\theta - 30^o) + \frac{2 \cdot dm \cdot \sin(\theta - 30^o)}{\sqrt{3}})$
$t_6 = T_s \cdot (-1 - \frac{4 \cdot dm \cdot \sin(\theta - 30^o)}{\sqrt{3}})$
$t_{61} = T_s \cdot (2 \cdot dm \cdot \cos(\theta - 30^o) + \frac{2 \cdot dm \cdot \sin(\theta - 30^o)}{\sqrt{3}})$

i=1, j=2
$t_{06} = T_s \cdot (1 - 2 \cdot dm \cdot \cos(\theta - 30^o) - \frac{2 \cdot dm \cdot \sin(\theta - 30^o)}{\sqrt{3}})$
$t_{01} = T_s \cdot (1 + \frac{4 \cdot dm \cdot \sin(\theta - 30^o)}{\sqrt{3}})$
$t_{61} = T_s \cdot (-1 + 2 \cdot dm \cdot \cos(\theta - 30^o) - \frac{2 \cdot dm \cdot \sin(\theta - 30^o)}{\sqrt{3}})$

i=1, j=3
$t_{01} = T_s \cdot (2 - 2 \cdot dm \cdot \cos(\theta - 30^o) + \frac{2 \cdot dm \cdot \sin(\theta - 30^o)}{\sqrt{3}})$
$t_{61} = T_s \cdot (-\frac{4 \cdot dm \cdot \sin(\theta - 30^o)}{\sqrt{3}})$
$t_1 = T_s \cdot (-1 + 2 \cdot dm \cdot \cos(\theta - 30^o) + \frac{2 \cdot dm \cdot \sin(\theta - 30^o)}{\sqrt{3}})$

i=1, j=4
$t_{01} = T_s \cdot (-\frac{4 \cdot dm \cdot \sin(\theta - 30^o)}{\sqrt{3}})$
$t_{02} = T_s \cdot (2 \cdot dm \cdot \cos(\theta - 30^o) + \frac{2 \cdot dm \cdot \sin(\theta - 30^o)}{\sqrt{3}})$
$t_0 = T_s - t_{01} - t_{02}$

APPENDIX C: SABER NETLIST OF THE THREE-LEVEL VSI

(This netlist is for power stage only.)

```
#########################################################################
#                                                                       #
# Saber netlist for three-level VSI                                     #
# Created by the Saber Integration Toolkit 3.4b-2.7b of Analogy, Inc.   #
# Created on November 23, 1996          .                               #
# Muhammet Cosan                                                        #
# Virginia Polytechnic Institute & State University                     #
#                                                                       #
#########################################################################

ide_tech..model  _ls=(voh=2.8,vol=0.4,vxh=2.2,vxl=0.8,
        tr=10n,tf=10n,tdon=20n,tdoff=20n)

ide_d2an.@"clock_l4#109_clock" a:clock d:@"clock_clock_l4#109_clock" m:0 = \model=_ls
ide_d2an.@"buf_l4#226_out" a:SS6 d:@"SS6_buf_l4#226_out" m:0 = model=_ls
ide_d2an.@"buf_l4#225_out" a:SS5 d:@"SS5_buf_l4#225_out" m:0 = model=_ls
ide_d2an.@"buf_l4#213_out" a:SS4 d:@"SS4_buf_l4#213_out" m:0 = model=_ls
ide_d2an.@"buf_l4#202_out" a:SS3 d:@"SS3_buf_l4#202_out" m:0 = model=_ls
ide_d2an.@"buf_l4#200_out" a:@"n#388" d:@"n#388_buf_l4#200_out" m:0 = model=_ls
ide_d2an.@"buf_l4#149_out" a:SS2 d:@"SS2_buf_l4#149_out" m:0 = model=_ls
ide_d2an.@"inv_l4#228_out" a:SS5p d:@"SS5p_inv_l4#228_out" m:0 = model=_ls
ide_d2an.@"inv_l4#227_out" a:SS6p d:@"SS6p_inv_l4#227_out" m:0 = model=_ls
ide_d2an.@"inv_l4#210_out" a:SS3p d:@"SS3p_inv_l4#210_out" m:0 = model=_ls
ide_d2an.@"inv_l4#205_out" a:SS4p d:@"SS4p_inv_l4#205_out" m:0 = model=_ls
ide_d2an.@"inv_l4#133_out" a:SS1p d:@"SS1p_inv_l4#133_out" m:0 = model=_ls
ide_d2an.@"inv_l4#75_out" a:SS2p d:@"SS2p_inv_l4#75_out" m:0 = model=_ls
v.@"v_dc#60" m:0 p:@"n#384" = dc=1800
r.Rxx m:0 p:y = rnom=2meg
r.@"rh#242" m:@"n#371" p:0 = rnom=1u
r.Ra m:y p:aa = rnom=4.6
r.Rb m:y p:bb = rnom=4.6
r.Rc m:y p:cc = rnom=4.6
r.Rx m:0 p:@"n#341" = rnom=2meg
l.Lc m:cc p:c = l=0.25m, r=1m
l.Lb m:bb p:b = l=0.25m, r=1m
l.La m:aa p:a = l=0.25m, r=1m
muh1.svm s1:1 s2:2 s3:3 s4:4 s5:5 s6:6 da:da db:db  # this is the SVM file
c.@"c#64" m:@"n#371" p:MIDPOINT = ic=900, c=1m
c.@"c#62" m:MIDPOINT p:@"n#384" = ic=900, c=1m
c.Ca m:@"n#341" p:aa = c=100u
c.Cb m:@"n#341" p:bb = c=100u
c.Cc m:@"n#341" p:cc = c=100u
c.@"c#319" m:@"n#38" p:@"n#384" = c=7n
c.@"c#320" m:b p:@"n#38" = c=7n
c.@"c#321" m:@"n#39" p:b = c=7n
```

```
c.@"c#322" m:@"n#371" p:@"n#39" = c=7n
c.@"c#323" m:@"n#371" p:@"n#280" = c=7n
c.@"c#324" m:@"n#280" p:a = c=7n
c.@"c#325" m:a p:@"n#278" = c=7n
c.@"c#326" m:@"n#278" p:@"n#384" = c=7n
c.@"c#327" m:@"n#37" p:@"n#384" = c=7n
c.@"c#328" m:c p:@"n#37" = c=7n
c.@"c#329" m:@"n#35" p:c = c=7n
c.@"c#330" m:@"n#371" p:@"n#35" = c=7n
vsine.vcos m:0 p:vcos = ph=90, ampl=0.8, f=60
vsine.vsin m:0 p:vsin = ampl=0.8, f=60
d.D2 n:MIDPOINT p:@"n#280"
d.D4 n:MIDPOINT p:@"n#39"
d.D6 n:MIDPOINT p:@"n#35"
d.D1 n:@"n#278" p:MIDPOINT
d.D3 n:@"n#38" p:MIDPOINT
d.D5 n:@"n#37" p:MIDPOINT
inv_l4.@"inv_l4#75" out:@"SS2p_inv_l4#75_out" in:2
inv_l4.@"inv_l4#133" out:@"SS1p_inv_l4#133_out" in:1
inv_l4.@"inv_l4#205" out:@"SS4p_inv_l4#205_out" in:4
inv_l4.@"inv_l4#210" out:@"SS3p_inv_l4#210_out" in:3
inv_l4.@"inv_l4#227" out:@"SS6p_inv_l4#227_out" in:6
inv_l4.@"inv_l4#228" out:@"SS5p_inv_l4#228_out" in:5
buf_l4.@"buf_l4#149" out:@"SS2_buf_l4#149_out" in:2
buf_l4.@"buf_l4#200" out:@"n#388_buf_l4#200_out" in:1
buf_l4.@"buf_l4#202" out:@"SS3_buf_l4#202_out" in:3
buf_l4.@"buf_l4#213" out:@"SS4_buf_l4#213_out" in:4
buf_l4.@"buf_l4#225" out:@"SS5_buf_l4#225_out" in:5
buf_l4.@"buf_l4#226" out:@"SS6_buf_l4#226_out" in:6
sw_vc.@"sw_vc#156" m:@"n#384" p:@"n#278" vm:0 vp:@"n#388" =
\model=(2,1m,0.1m,10meg)
sw_vc.@"sw_vc#159" m:@"n#278" p:a vm:0 vp:SS2p = model=(2,1m,0.1m,10meg)
sw_vc.@"sw_vc#160" m:a p:@"n#280" vm:0 vp:SS1p = model=(2,1m,0.1m,10meg)
sw_vc.@"sw_vc#161" m:@"n#280" p:@"n#371" vm:0 vp:SS2 = model=(2,1m,0.1m,10meg)
sw_vc.@"sw_vc#165" m:@"n#39" p:@"n#371" vm:0 vp:SS4 = model=(2,1m,0.1m,10meg)
sw_vc.@"sw_vc#166" m:b p:@"n#39" vm:0 vp:SS3p = model=(2,1m,0.1m,10meg)
sw_vc.@"sw_vc#167" m:@"n#38" p:b vm:0 vp:SS4p = model=(2,1m,0.1m,10meg)
sw_vc.@"sw_vc#168" m:@"n#384" p:@"n#38" vm:0 vp:SS3 = ic=on, \model=(2,1m,0.1m,10meg)
sw_vc.@"sw_vc#172" m:@"n#35" p:@"n#371" vm:0 vp:SS6 = model=(2,1m,0.1m,10meg)
sw_vc.@"sw_vc#173" m:c p:@"n#35" vm:0 vp:SS5p = model=(2,1m,0.1m,10meg)
sw_vc.@"sw_vc#174" m:@"n#37" p:c vm:0 vp:SS6p = model=(2,1m,0.1m,10meg)
sw_vc.@"sw_vc#175" m:@"n#384" p:@"n#37" vm:0 vp:SS5 = model=(2,1m,0.1m,10meg)
sh.@"sh#101" out:db in:vsin gate:clock gnd:0
sh.@"sh#114" out:da in:vcos gate:clock gnd:0
clock_l4.@"clock_l4#109" clock:@"clock_clock_l4#109_clock" = freq=40000, duty=0.5
```

APPENDIX D: COMPLETE SVM ALGORITHM

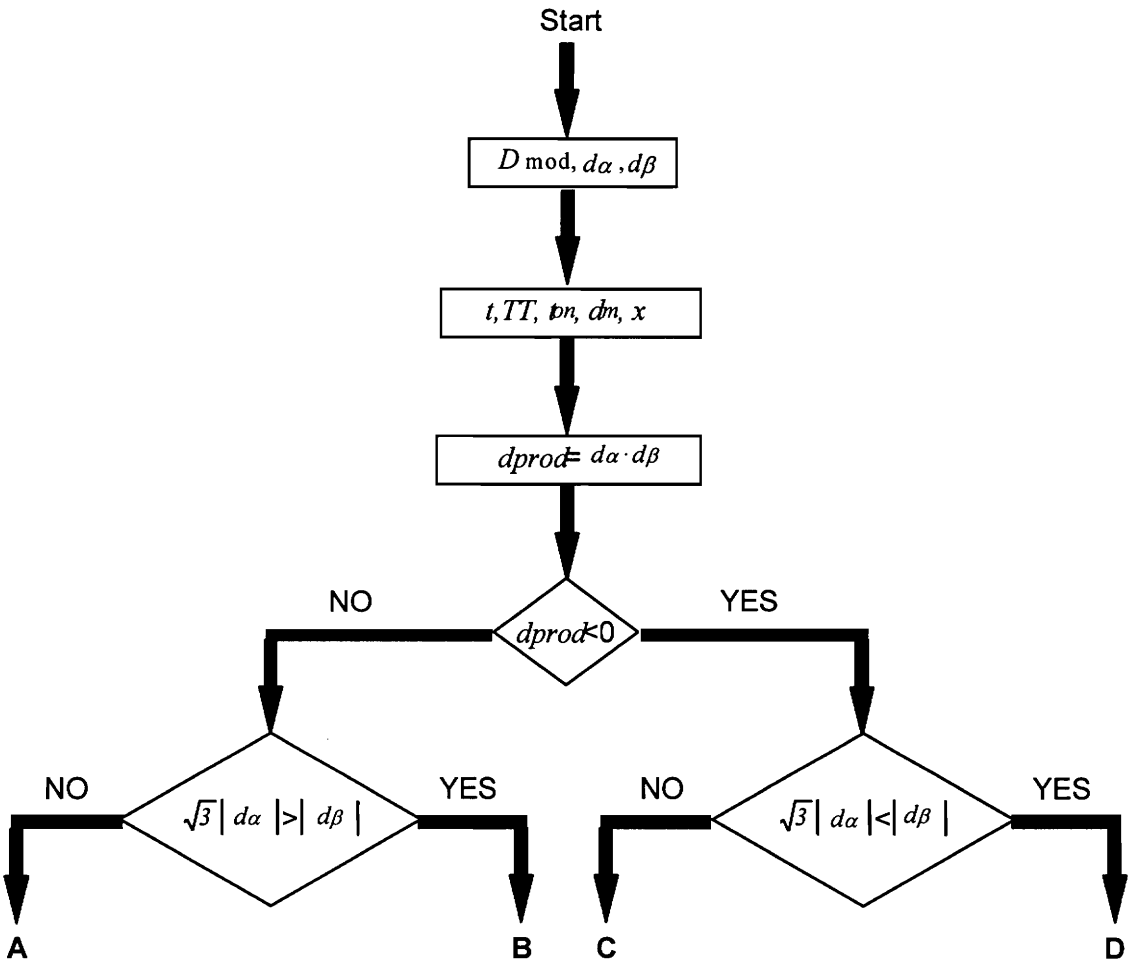

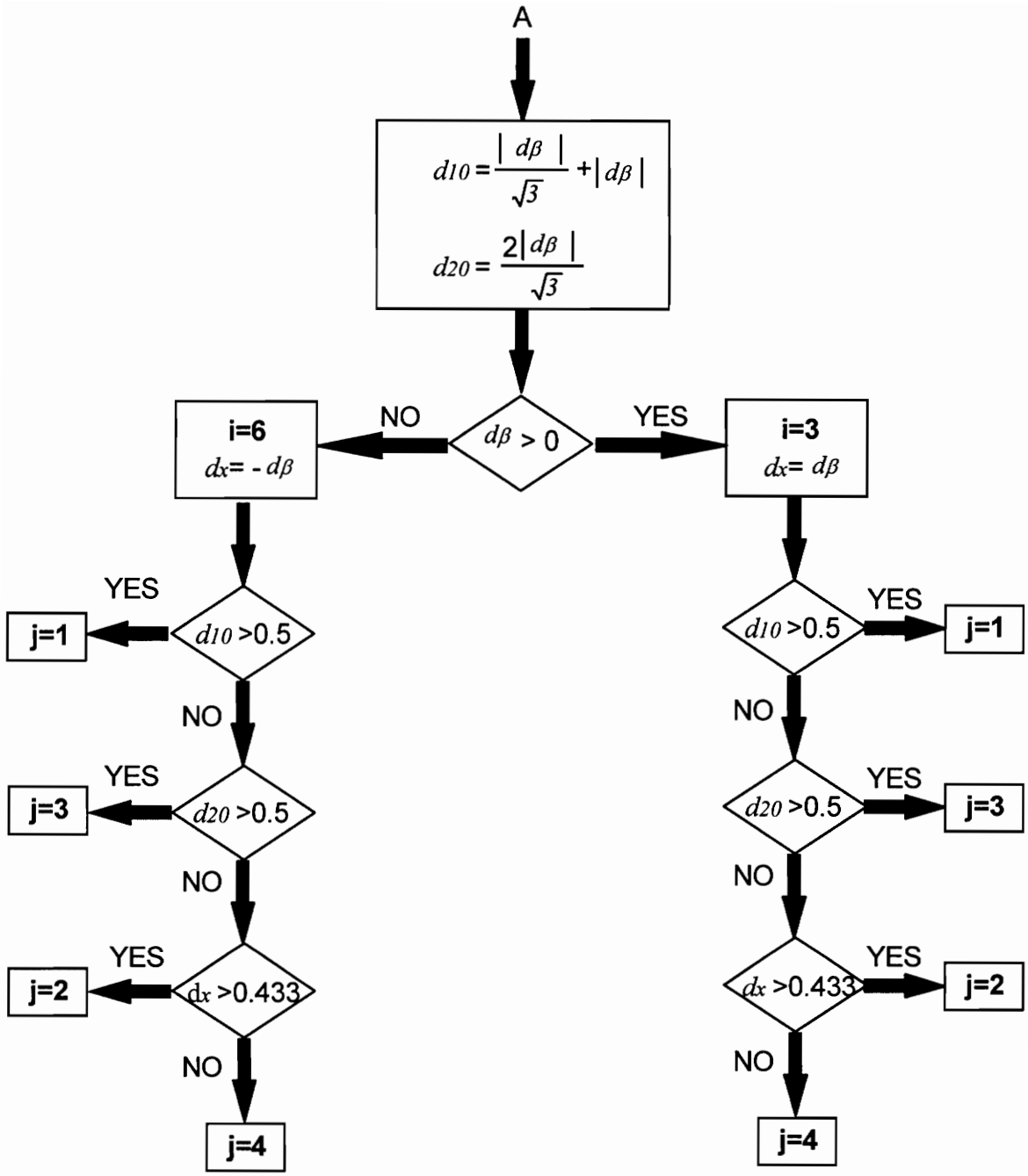
A
$d10 = \frac{|d\beta|}{\sqrt{3}} + |d\beta|$
$d20 = \frac{2|d\beta|}{\sqrt{3}}$
$d\beta > 0$
NO
YES
i=6
$dx = -d\beta$
i=3
$dx = d\beta$
$d10 > 0.5$
YES
j=1
NO
$d20 > 0.5$
YES
j=3
NO
$dx > 0.433$
YES
j=2
NO
j=4
$d10 > 0.5$
YES
j=1
NO
$d20 > 0.5$
YES
j=3
NO
$dx > 0.433$
YES
j=2
NO
j=4

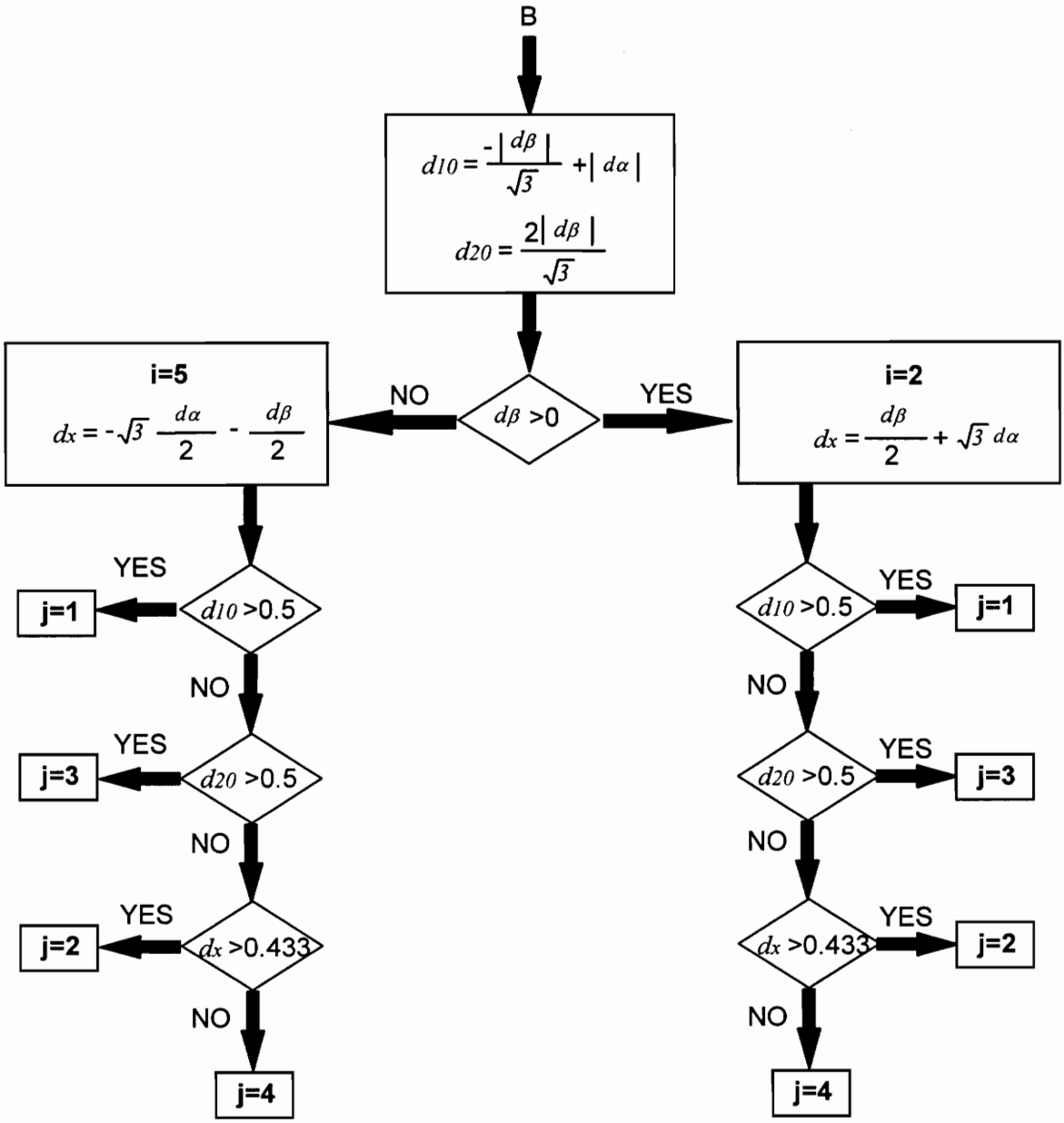
B
$d10 = \frac{-|d\beta|}{\sqrt{3}} + |d\alpha|$
$d20 = \frac{2|d\beta|}{\sqrt{3}}$
$d\beta > 0$
NO
YES
i=5
$dx = -\sqrt{3}\frac{d\alpha}{2} - \frac{d\beta}{2}$
i=2
$dx = \frac{d\beta}{2} + \sqrt{3}\,d\alpha$
$d10 > 0.5$
YES
j=1
NO
$d20 > 0.5$
YES
j=3
NO
$dx > 0.433$
YES
j=2
NO
j=4
$d10 > 0.5$
YES
j=1
NO
$d20 > 0.5$
YES
j=3
NO
$dx > 0.433$
YES
j=2
NO
j=4

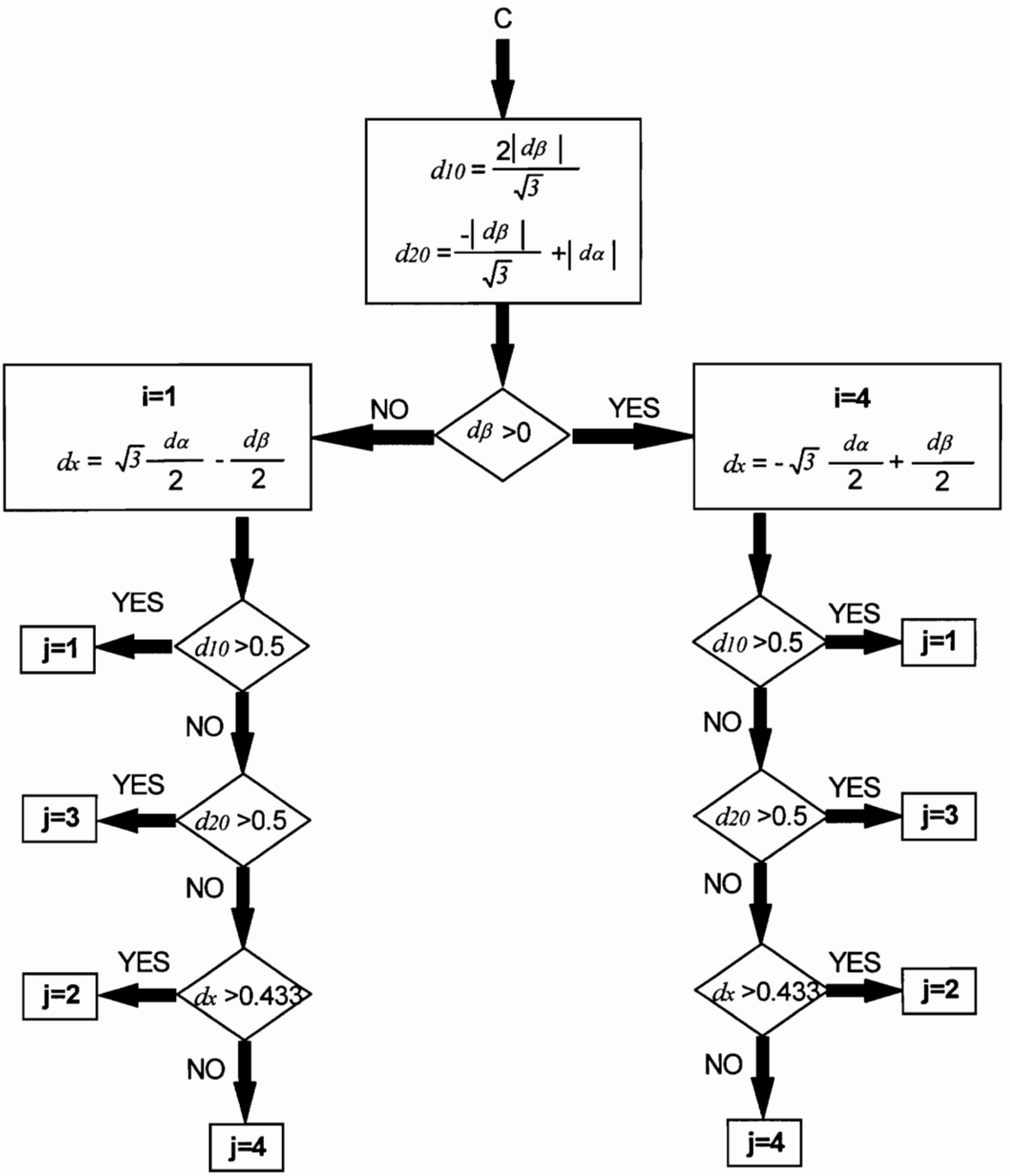
C
$d10 = \frac{2|d\beta|}{\sqrt{3}}$
$d20 = \frac{-|d\beta|}{\sqrt{3}} + |d\alpha|$
$d\beta > 0$
NO
YES
i=1
$dx = \sqrt{3}\frac{d\alpha}{2} - \frac{d\beta}{2}$
i=4
$dx = -\sqrt{3}\frac{d\alpha}{2} + \frac{d\beta}{2}$
$d10 > 0.5$
YES
j=1
NO
$d20 > 0.5$
YES
j=3
NO
$dx > 0.433$
YES
j=2
NO
j=4
$d10 > 0.5$
YES
j=1
NO
$d20 > 0.5$
YES
j=3
NO
$dx > 0.433$
YES
j=2
NO
j=4

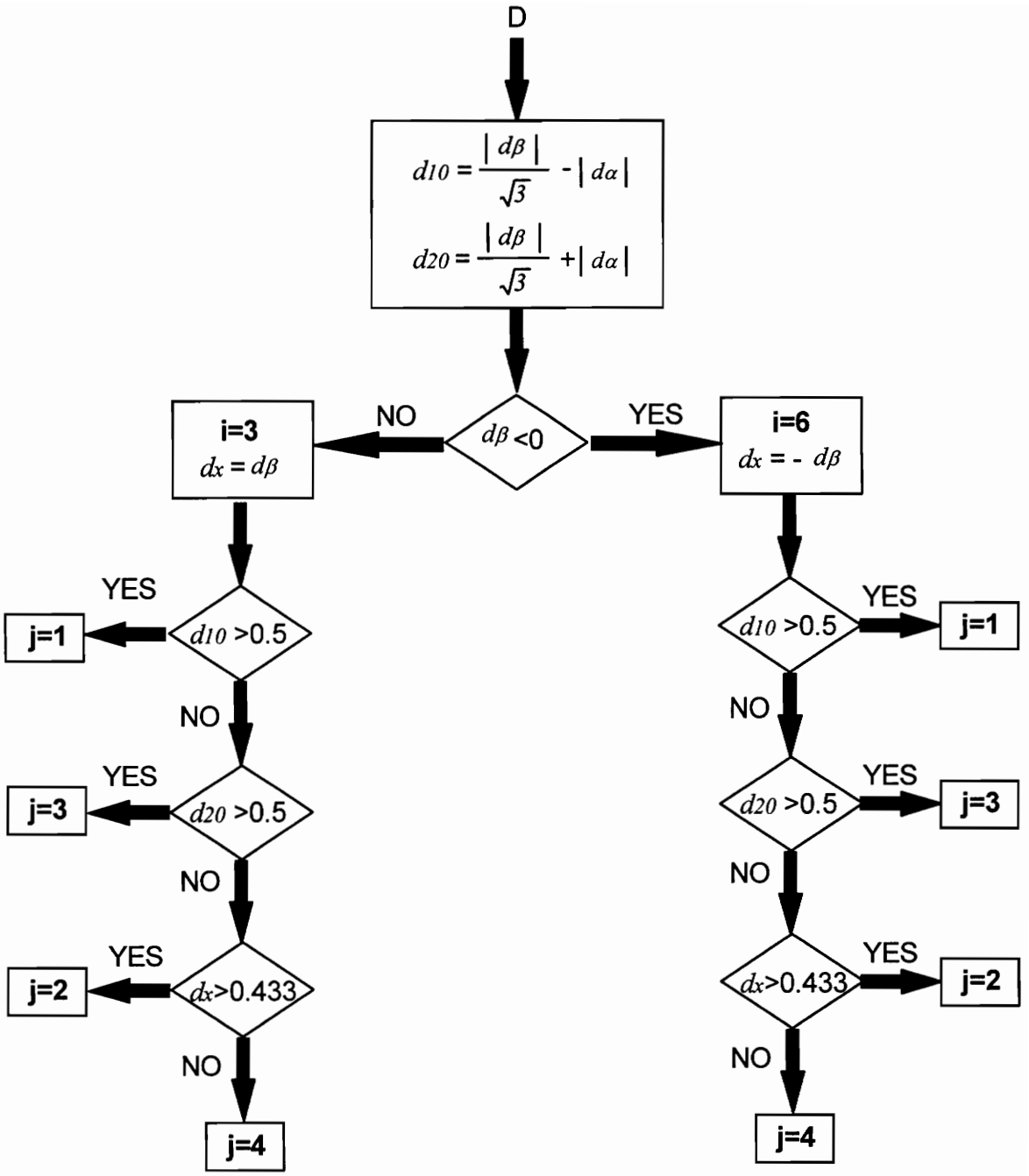
D
$d10 = \frac{|d\beta|}{\sqrt{3}} - |d\alpha|$
$d20 = \frac{|d\beta|}{\sqrt{3}} + |d\alpha|$
$d\beta < 0$
NO
YES
i=3
$dx = d\beta$
i=6
$dx = -d\beta$
$d10 > 0.5$
YES
j=1
NO
$d20 > 0.5$
YES
j=3
NO
$dx > 0.433$
YES
j=2
NO
j=4
$d10 > 0.5$
YES
j=1
NO
$d20 > 0.5$
YES
j=3
NO
$dx > 0.433$
YES
j=2
NO
j=4

APPENDIX E: TRANSFER FUNCTIONS

vp/dpd transfer function

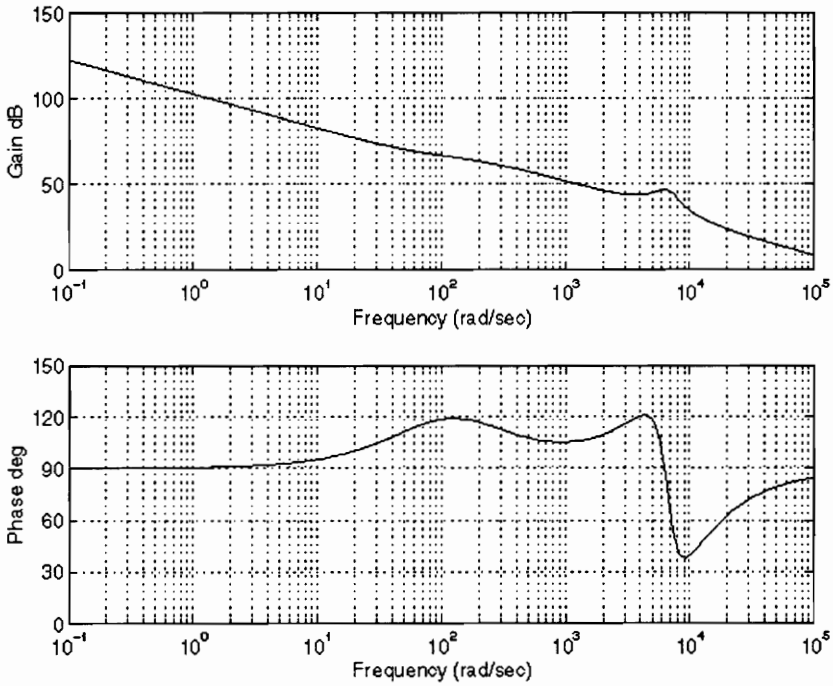

Vpn/dpd transfer function

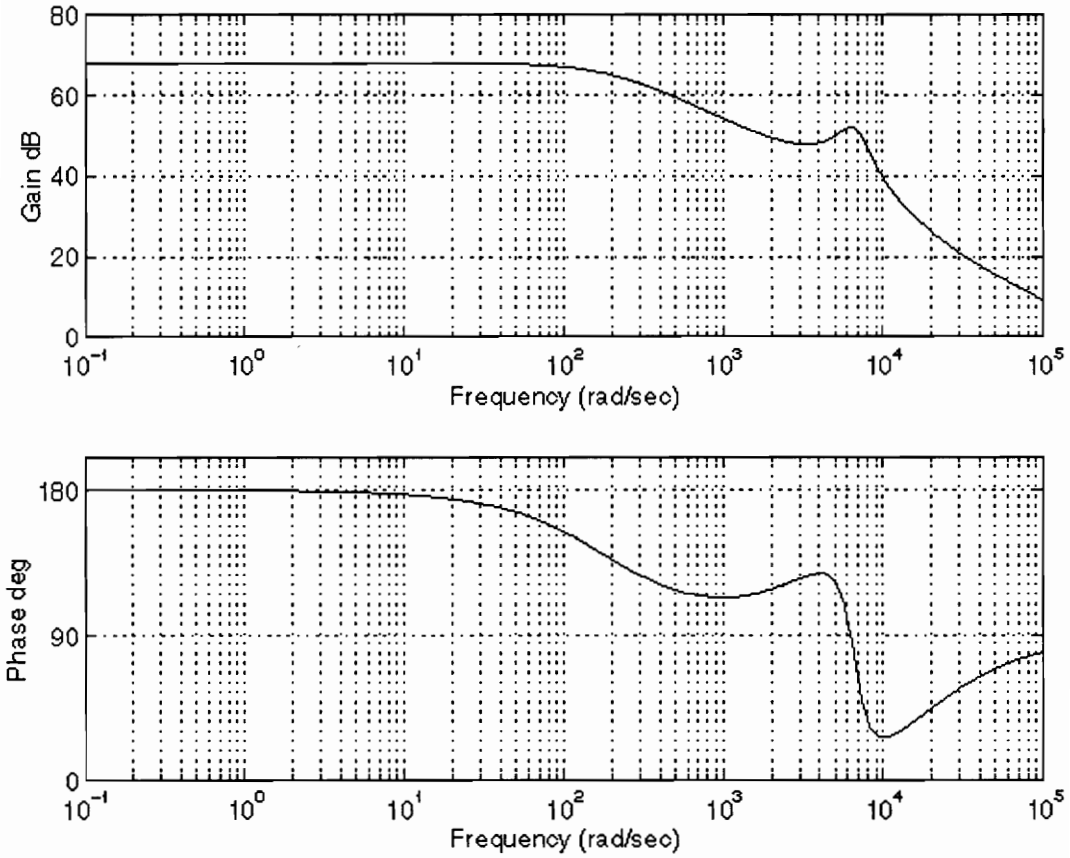

APPENDIX F: SIMULATION OF D-Q-0 MODEL BY PSPICE

Schematics of the PSPICE simulation circuit:

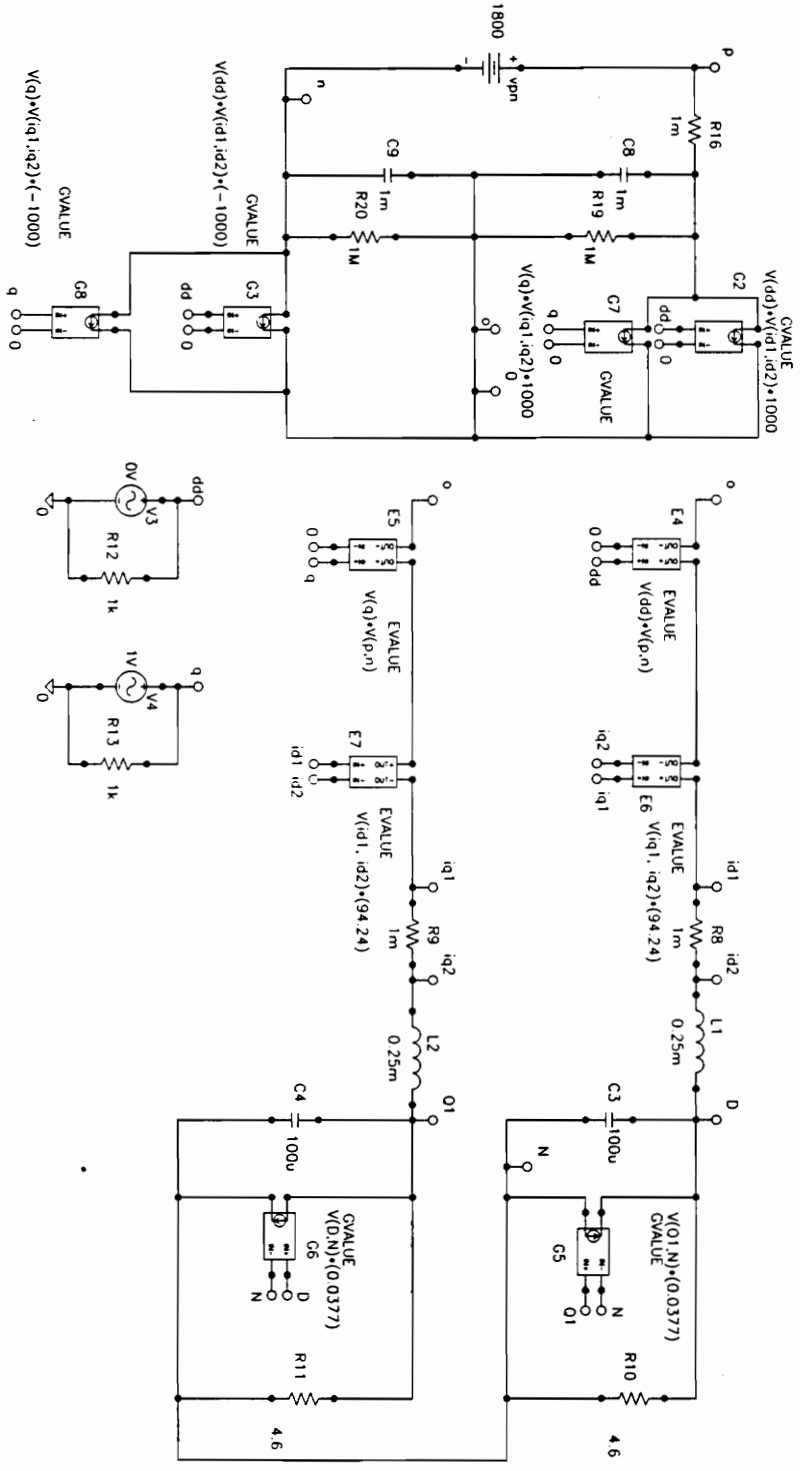

* Schematics Netlist *

```
R_R8       id1 id2  1m
E_E6       id1 $N_0001 VALUE { V(iq1, iq2)*(94.24) }
E_E7       $N_0002 iq1 VALUE { V(id1, id2)*(94.24) }
G_G6       Q1 N VALUE { V(D,N)*(0.0377) }
R_R10       N D  4.6
R_R11       N Q1  4.6
C_C3       N D  100u
C_C4       N Q1  100u
L_L1       id2 D  0.25m
V_vpn       p N 1800
L_L2       iq2 Q1  0.25m
R_R9       iq1 iq2  1m
C_C8       0 $N_0003  1m
C_C9       N 0  1m
R_R16       p $N_0003  1m
R_R19       0 $N_0003  1M
R_R20       N 0  1M
R_R13       0 q  1k
R_R12       0 dd  1k
G_G2       $N_0003 0 VALUE { V(dd)*V(id1,id2)*1000 }
G_G3       N 0 VALUE { V(dd)*V(id1,id2)*(-1000) }
E_E4       $N_0001 0 VALUE { V(dd)*V(p,N) }
E_E5       $N_0002 0 VALUE { V(q)*V(p,N) }
G_G8       N 0 VALUE { V(q)*V(iq1,iq2)*(-1000) }
G_G7       $N_0003 0 VALUE { V(q)*V(iq1,iq2)*1000 }
G_G5       N D VALUE { V(Q1,N)*(0.0377) }
V_V3       dd 0 DC 0.7V AC 0V
V_V4       q 0 DC 0.0145V AC 1V
```

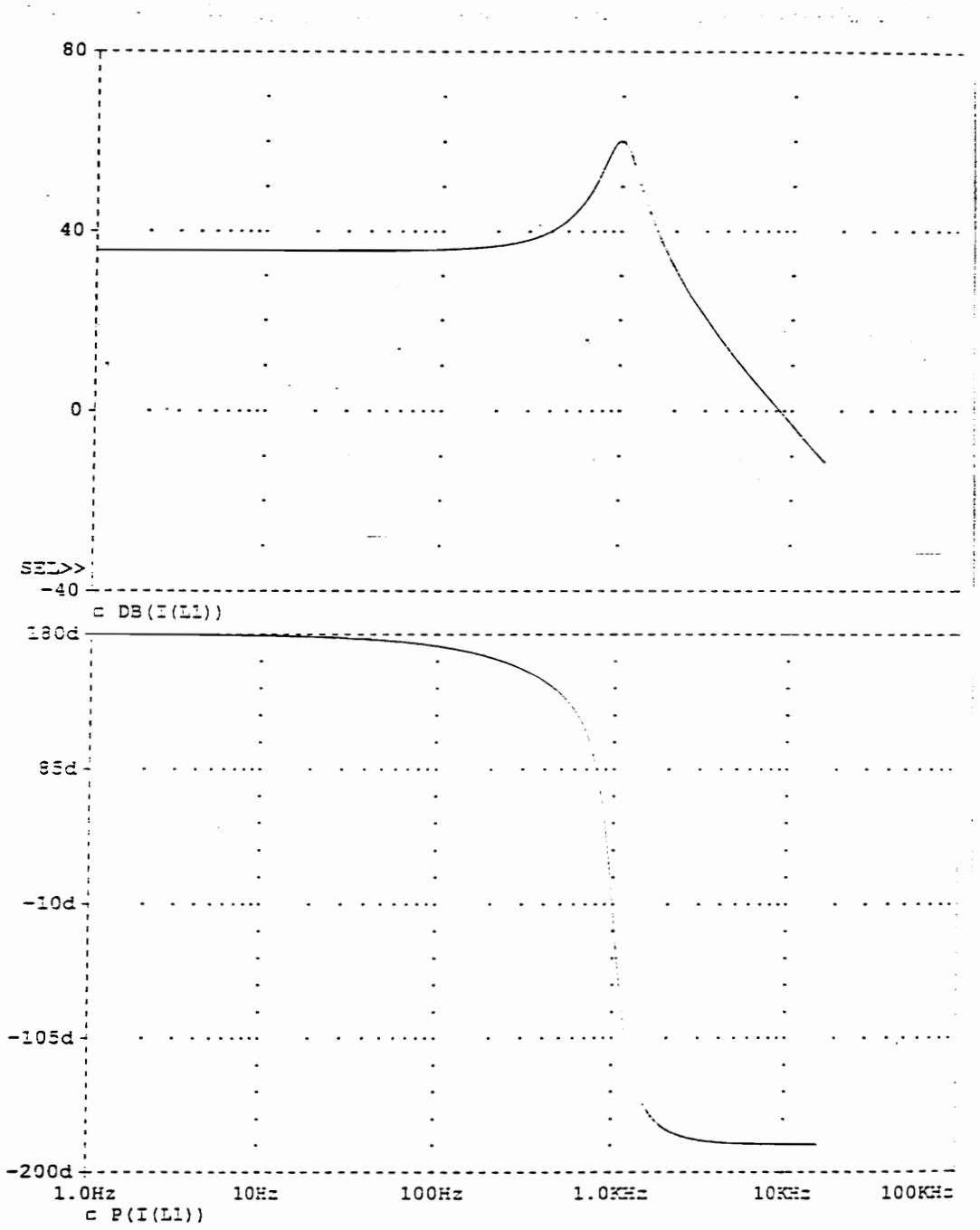

Simulation result of $\hat{i}_{Yd}/\hat{d}_{pq}$.

REFERENCES

[1] A. Nabae, I. Takahashi and H. Akagi, "A New Neutral-Point-Clamped PWM Inverter", IEEE Trans. Ind. Appl., vol IA-17, no 5, pp. 518-523, 1981

[2] J. Lai, F. Z. Peng, "Multilevel Converters- A New Breed of Power Converters",IEEE IAS Conf. Rec., pp. 2348-2356, 1995

[3] K. Shimane, and Y. Nakazawa, " Harmonic Reduction for NPC Converter with a New Scheme", IPEC Conf. Rec., 1995, pp. 482-87.

[4] H. Mao, D. Borojevic, and F. C. Lee, "Multi-level 2-quadrant Boost Chopper for Superconductive Magnetic Energy Storage", IEEE APEC Conf. Rec., 1996, 876-882.

[5] Analogy Inc., "Design Star User Manual".

[6] Analogy Inc., "Guide to Writing Templates".

[7] Khai D. Ngo, "Low Frequency Characterization of PWM Converters", IEEE Trans. On Power Electronics , vol. PE-1, no. 4, pp. 223-230, October 1986.

[8] V. Vlatkovic, D. Borojevic, and F. C. Lee, "Soft-transition Three-phase PWM Conversion Technology, " PESC-94 Conf. Rec., pp. 79-84.

[9] S. Ogosawara, and H. Akagi, "Analysis of Variation of Neutral Point Potential in NPC Voltage Source Inverter," IEEE-IAS Conf. Rec., pp. 965-970, 1993

[9] G. C. Cho, G. H. Jung, N. S. Choi, and G. H. Cho, " Analysis and Controller Design of a Static Var Compensator Using Three-level GTO Inverter", IEEE Trans. On Power Electronics, vol. 11, no. 1, pp. 57-65 January 1996.

[10] Silva Hiti, "Modeling and Control of Three-phase PWM Converters,", Ph.D. Dissertation, Virginia Polytechnic Institute and State University, Blacksburg, VA, 1995.

[11] J. Bordonau, M. Cosan, D. Borojevic, H. Mao, and F. C. Lee, "A State-space Model For The Comprehensive Dynamic Analysis of Three-level Voltage-source Inverters", IEEE, PESC Conf. Rec. 1997, pp. 942-948.

[12] J. Xu, "Modeling of Switching dc-dc Converters by Time-averaging Equivalent Circuit Approach," Int. J. Electronics, vol. 74 no. 3, 1993

[13] Evaluation version of PSPICE 7.1, MicroSim DesignLab.

Vita

Muhammet Cosan was born in Kocaeli, Turkey in 1971. He received his Bachelor of Science degree with honors in electrical engineering from Istanbul Technical University, Istanbul, Turkey, in 1992.

He joined Virginia Power Electronics Center (VPEC) in the spring of 1995 as a graduate research assistant. He was involved in research at VPEC in the areas of space vector modulation techniques, modeling and control of switching power converters. His area of interest includes soft switching techniques, multi-level converters and high-power applications. He is currently a design engineer with York International Corp., York, PA.